Powder Technology 437 (2024) 119526

Contents lists available at ScienceDirect

Powder Technology

journal homepage: www.journals.elsevier.com/powder-technology

Coefficient of tangential restitution for non-spherical particles

Jana Wedel [a,*], Matjaž Hriberšek [b], Paul Steinmann [a,c], Jure Ravnik [b]

[a] Institute of Applied Mechanics, Friedrich-Alexander Universität Erlangen-Nürnberg, Paul-Gordan-Str. 3, D-91052 Erlangen, Germany
[b] Faculty of Mechanical Engineering, University of Maribor, Smetanova 17, SI-2000, Maribor, Slovenia
[c] Glasgow Computational Engineering Centre, University of Glasgow, Glasgow, UK

GRAPHICAL ABSTRACT

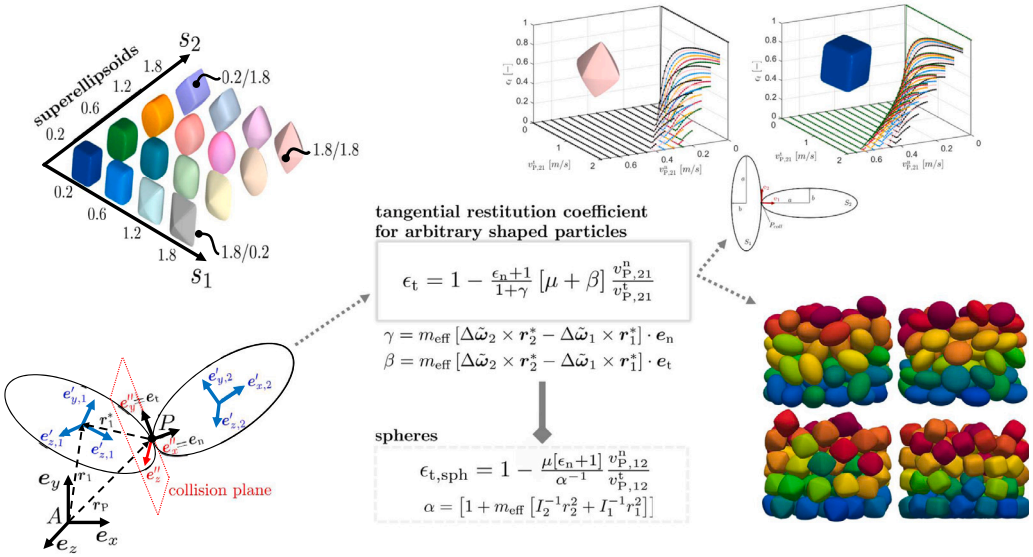

HIGHLIGHTS

- Tangential restitution coefficient ϵ_t model for arbitrary shaped particles was presented.
- The novel ϵ_t model is in agreement with literature results for sperical shapes.
- The impact of relative normal and relative tangential collision velocity on ϵ_t was analyzed.
- The impact of superellipsoidal shape factors on ϵ_t was investigated.
- Cylinder filling process using various superellipsoidal shapes were computed.

ARTICLE INFO

Keywords:
Non-spherical particles
Particle collision
Tangential restitution coefficient

ABSTRACT

In various industrial and naturally occurring multiphase flows, whether dilute or dense, particle interaction plays a crucial role. In most cases, the particles are non-spherical, which poses a computational challenge in terms of particle motion and particle interaction, i.e. both particle–particle and particle–wall collisions.

* Corresponding author.
E-mail addresses: jana.wedel@fau.de (J. Wedel), matjaz.hribersek@um.si (M. Hriberšek), paul.steinmann@fau.de (P. Steinmann), jure.ravnik@um.si (J. Ravnik).

https://doi.org/10.1016/j.powtec.2024.119526
Received 11 December 2023; Received in revised form 1 February 2024; Accepted 8 February 2024
Available online 9 February 2024

Superellipsoids

In this study, we present a novel frictional particle collision model to be used in general fluid flows. The model is derived for superellipsoidal particle shapes and thus allows consideration of frictional collisions of a wide variety of particle geometries. In this context, we derive an expression for the tangential coefficient of restitution applicable to arbitrarily shaped particles. Furthermore, we present the performance of the novel model by applying it to demonstrative examples ranging from two- to multi-particle systems.

1. Introduction

Accurate modeling of the physics of complex particulate systems is of key interest to various industries such as pharmaceuticals, petrochemicals, and wastewater treatment, [1,2], as a better understanding can help increase the efficiency of such applications. In targeted drug delivery, for example, better knowledge of particle behavior can be used to reduce side effects as well as increase the drug efficacy, [3]. It should be noted that naturally occurring and man-made particles are rarely perfectly spherical, such as blood cells, dust particles, or fibers, which contributes to the increased complexity of particle motion. In addition, the description of particle–particle and particle–wall collisions becomes more complex when the particle shapes deviate from spherical. Another complication is the consideration of friction in particle–particle and particle–wall collisions, which is often neglected, although it can significantly impact the post-collisional movement of particles.

In the literature, there are a variety of approaches that target non-spherical particles in collision problems, such as the polygon formulation, [4,5], discrete function representation (DFR), [6,7], continuous function representation (CFR), [7–9], and composite particles. Hogue and Newland, [4] investigated falling dominoes using the polygon formulation. The authors obtained good agreement with experimental results. In addition, Feng and Owen, [5], investigated 2D polygon collisions and proposed a contact model for corner contacts. Another method to account for non-sphericity is the CFR method, in which the particle surface is expressed in a continuous fashion by employing a surface equation such as the superellipsoidal surface equation, [9]. Mustoe and Miyata, [10] used the CFR method in combination with the superellipsoid surface equation to study cube-shaped particles in a horizontal, rotating 2D cylinder, focusing on the relationship between the particle squareness and the dynamic angle of response. It is well known that the CFR method has significant convergence problems as the squareness of the particles increases, [1]. In contrast to CFR, the DFR method, [6], models the particle surface with a chosen number of discrete points and is a reasonable alternative to CFR due to its lower computational cost and applicability to a large variability of particle shapes, [11]. Note that a suitable number of points must be chosen for accurate shape representation and collision resolution, with the computational cost of the DRF method increasing with the number of surface nodes N as $\mathcal{O}(N)$. Another commonly used modeling technique is the multi-sphere composite approach, [12,13], in which a set of prime spheres is combined to approximate arbitrary shapes, [7]. Abbaspour-Fard [14], describes the efficiency of contact detection, as it is reduced to sphere-sphere contact detection, and the comparatively simple implementation as the main advantages of the multi-sphere approximation. A disadvantage of the multi-sphere approach is the strong dependence on the number of prime spheres used to represent the surface. Thus, for complex particle shapes, a high number of spheres is usually required to obtain a sufficiently smooth surface representation, which leads to high computational costs, [7]. Moreover, approximating a convex shape such as ellipsoids or superellipsoids by a set of spheres leads to a non-convex shape and consequently to the occurrence of multiple contact points, [7].

In our previous work, [9], we discussed various techniques to account for nonsphericity of particles, such as polygon-shaped particles, multisphere composites, discrete function representation (DFR), and continuous function representation (CFR), where the last one proved to be superior in the scope of our work. In this context our previous work, [9], presented a novel frictional particle–wall and particle–particle collision model, applicable to any superellipsoidal particle collisions occurring in flows. The method proved to be efficient and robust even in the case where non-binary particle contacts occur, for example in filling processes, where a particle can be in contact with various other particles as well as the container wall. The method is based on a Lagrangian multiplier optimization technique in combination with the Newton–Raphson method, [9]. As no discretization of the particle surface is required, the approach is able to consider multitude of particles ($\mathcal{O} > 10^5$) during thousands of time steps, [9].

To evaluate the loss of mechanical energy in particle systems due to particle–particle as well as particle–wall collisions, the normal and tangential coefficients are commonly used, [15,16]. The normal and tangential restitution coefficients relate the normal and tangential post- and pre-collisional relative velocities, respectively, [17]. Most expressions for ϵ_n and ϵ_t are derived only for sphere-sphere and sphere-wall interactions since the particle shape simplifies the collision problem considerably. Therefore, various experiments and models targeting the restitution coefficients for spherical particles can be found in the literature, [16–18]. Bridges et al. experimentally investigated ϵ_n for spherical ice particles in plane wall collisions, [19–21]. The authors observed the dependence of ϵ_n on a variety of parameters such as particle diameter, surface roughness, and temperature. In addition, Schwager and Pöschel, [15], proposed an analytical expression for ϵ_n by studying viscous spherical particles, improving Bridger's model where the ϵ_n can become infinite with decreasing impact velocities. The derivation of models for restitution coefficients for arbitrary particle shapes has long been studied, [22], and remains a challenge as they are influenced not only by particle material, size, and relative impact velocity but also by particle shape and contact inclination angle due to their non-sphericity, [16]. Hu et al. [16], experimentally investigated ϵ_n for spheres and simple non-spherical particles, i.e. prolate ellipsoids, in wall collisions and provided experimental measurements. The authors showed that ϵ_n has both translational and rotational contributions. The authors also found that near a pole the translational contribution is dominant, while near the particle equator, the rotational contribution is major, indicating that the contributions depend significantly on the position of the contact point. Huang et al. [23], proposed a simplified 2D collision model to describe ϵ_n for prolate ellipsoids in wall collisions. The authors based their model on experiments as well as on momentum and angular momentum laws, [23]. Note that for the frictional collision of particles, the tangential restitution coefficient ϵ_t is additionally required. Becker et al. [18] investigated several ϵ_t models that apply to spheres. However, to capture the frictional particle collision for arbitrarily shaped particles, a more complex expression for ϵ_t is required which accounts for the nonspherical shape. Gui et al. [24] proposed a particle–wall collision model for non-spherical rigid particles in wall collisions assuming Coulomb friction.

In this work, we derive an expression for the tangential restitution coefficient assuming Coulomb friction for arbitrarily shaped particles. This work serves as an extension to our previously presented superellipsoid particle interaction model based on a hard-sphere collision technique, [9,25]. Combining our previously presented superellipsoid force models (see [25]) and our novel frictional particle–particle as well as particle–wall collisions approach, we are able to simulate the motion of suspended non-spherical particles, i.e. trajectories and rotations as well as frictional collisions.

This work is organized as follows: In Section 2, the particle collision approach, the collision frame, and the restitution coefficients

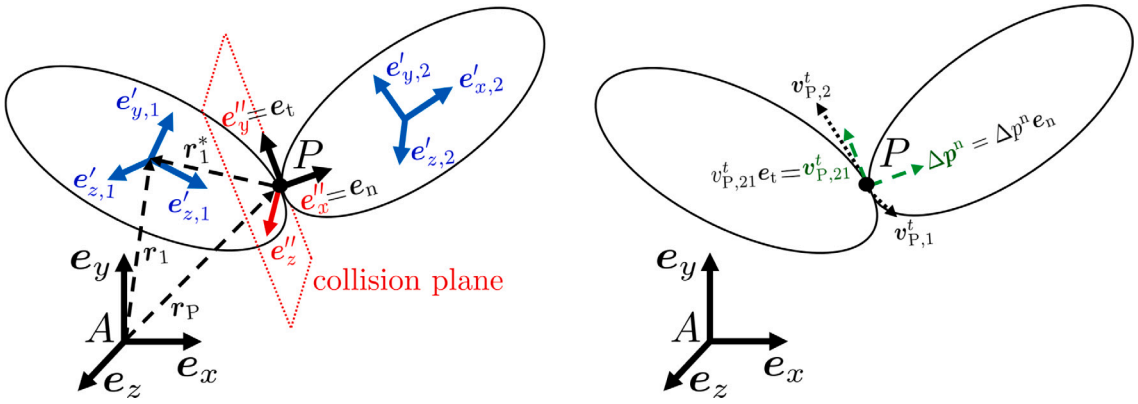

Fig. 1. Two superellipsoidal particles undergoing collision. Without loss of generality, we assume in the following that e_n points in the direction of the change of normal momentum. Furthermore, e_t is chosen to point in the direction of the relative tangential velocity of the contact point $v^t_{P,21} = v^t_{P,2} - v^t_{P,1}$.

are described. In Section 3, we discuss the conservation equations in superellipsoid–superellipsoid as well as superellipsoid–wall collisions. In Section 4, we derive an expression for the tangential restitution coefficient for arbitrary particle shapes. Furthermore, Section 5 contains the validation and demonstrative examples of superellipsoid–wall and superellipsoid–superellipsoid collisions based on the proposed method, followed by the main conclusions drawn from the study in Section 6.

2. Particle collision model

The particle collision model including contact point detection is based on our previous work, see Wedel et al. [9]. Here, we present a novel expression for the tangential restitution coefficient ϵ_t applicable to arbitrary particle shapes.

Notation: The notation employed in the scope of this study is in agreement with our preceding work, see Wedel et al. [9]. For convenience the notation can be found in Appendix A.

2.1. The collision frame of reference

We choose a collision frame of reference (cFoR) to simplify the consideration as much as possible. The collision frame originates at the contact point P and its unit basis vector e_x'' is aligned with the direction of the collision normal e_n, i.e. the identified surface normal at that contact point. The orthogonal unit basis vector e_y'' can be further aligned with e_t, the tangential unit vector pointing in the direction of the relative tangential velocity at the collision point. The third orthogonal unit basis vector can be obtained by $e''_z = e''_x \times e''_y$. The collision frame is depicted in Fig. 1.

Since we are considering a binary collision, we determine for the two colliding particles their position vectors relative to the collision point $r^*_\varphi = r_\varphi - r_P$, $\varphi = 1, 2$, (where r_φ denotes the position vector of particle φ and r_P labels the position vector of the contact point P). Their angular velocities are denoted as ω_φ and the particle orientations are captured in terms of their Euler parameters collected in $\underline{e}$. All physical quantities defined in the global frame $[\underline{r}^*_\varphi, \underline{v}_\varphi]$ and the body reference frame $[\underline{\omega}'_\varphi, \underline{I}_\varphi{}']$ must first be represented in the chosen collision frame $[x'', y'', z'']$. We transform the parameters of the global frame e_i to the cFoR e''_i by employing the global rotation matrix R_0. Furthermore, we transform the parameters of the body frame to the collision frame by using the body rotation matrices $\underline{R}_\varphi$, which transforms from the fixed body reference frame $e'_{i,\varphi}$ of the φ-th particle to the cFoR e''_i. Thus, we obtain the following relations:

$$\underline{r}''_\varphi = \underline{R}_0\,\underline{r}^*_\varphi, \qquad \underline{v}''_\varphi = \underline{R}_0\,\underline{v}_\varphi, \qquad \underline{\omega}''_\varphi = \underline{R}_\varphi\,\underline{\omega}'_\varphi, \qquad \underline{I}''_\varphi = \underline{R}_\varphi\,\underline{I}'_\varphi\,\underline{R}^{\mathrm{T}}_\varphi. \tag{1}$$

2.2. Coefficients of restitution

The frictional particle–particle and particle–wall interactions not only change the normal relative velocity, but also influence the tangential relative velocity, [18]. The relative velocity of particle "1" and "2" in the contact point is obtained using

$$v_{P,21} = v_{P,2} - v_{P,1}\,. \tag{2}$$

The relative velocity in the collision normal direction can be written as: [17]

$$v^n_{P,21} = \left[e_n \cdot v_{P,21}\right] e_n = v^n_{P,21} e_n\,, \tag{3}$$

where e_n denotes the collision normal. Without loss of generality, we assume in the following that e_n points in the direction of the change of normal momentum Δp^n, see below. The projection to the tangential plane results in:

$$v^t_{P,21} = e_n \times \left[e_n \times v_{P,21}\right] = v_{P,21} - v^n_{P,21} = \left[e_t \cdot v_{P,21}\right] e_t = v^t_{P,21} e_t\,, \tag{4}$$

where the direction of the tangential relative velocity is defined by the unit vector e_t. The (signed) length of the tangential relative velocity $v^t_{P,21}$ and the normal relative velocity $v^n_{P,21}$ are respectively obtained as follows:

$$v^t_{P,21} = v_{P,21} \cdot e_t\,, \qquad v^n_{P,21} = v_{P,21} \cdot e_n\,. \tag{5}$$

Note that by definition, $v^t_{P,21}$ is non-negative ($v^t_{P,21} \geq 0$) as $e_t = v^t_{P,21}/\|v^t_{P,21}\|$, [17].

A collision may be described by the coefficients of restitution, i.e. the normal restitution coefficient ϵ_n and the tangential restitution coefficient ϵ_t. The restitution coefficients relate the post- and pre-collisional values of the normal and tangential relative velocity, respectively.

The normal restitution coefficient ϵ_n relates the post- ($c^n_{p,21}$) and pre-collisional ($v^n_{p,21}$) values of the normal relative velocity as

$$\epsilon_n \equiv -\frac{c^n_{p,21}}{v^n_{p,21}}\,. \tag{6}$$

As indicated by Eq. (6), we identify that the normal restitution coefficient is defined in the range $0 \leq \epsilon_n \leq 1$, where $\epsilon_n = 0$ denotes a fully plastic collision and $\epsilon_n = 1$ a fully elastic collision wherein the normal velocity is conserved (with reversed sign), [18]. In general, ϵ_n can depend on the particle material parameters, the mass, the particle size as well as the relative impact velocity, [18]. As stated by Becker et al. [18], the assumption of a constant ϵ_n is commonly employed in molecular dynamics simulations, especially in the fields of granular systems. The author further concludes that the linear dashpot model is a force model leading to ϵ_n = constant. Consequently, ϵ_n depends only on material parameters and is independent of the relative impact velocity.

The linear dashpot force model is frequently employed in molecular dynamics simulations, see [26–36]. Nevertheless, we want to note that there are various force models available in the literature, which can lead to ϵ_n depending on the impact velocity, see for example [15,26,37–44], however, increasing the complexity of the collision description.

Becker et al. [18], stated that the assumption of a constant ϵ_n neither agrees in 2D nor in 3D perfectly with physical reality, yet it is justified as it simplifies the analysis of kinetic and hydrodynamic equations significantly, [18]. As the assumption of a constant ϵ_n is accepted for various applications, [18], we employ this limitation in the following.

Note that for the collision of frictional particles, we additionally need to account for the change of relative tangential velocity. The tangential restitution coefficient ϵ_t relates the post- ($c^\mathrm{t}_{\mathrm{P},21}$) and pre-collisional ($v^\mathrm{t}_{\mathrm{P},21}$) values of the tangential relative velocity as

$$\epsilon_\mathrm{t} \equiv +\frac{c^\mathrm{t}_{\mathrm{P},21}}{v^\mathrm{t}_{\mathrm{P},21}}\,. \tag{7}$$

The tangential restitution coefficient ϵ_t is in general defined in the range $-1 \le \epsilon_\mathrm{t} \le 1$, whereby the case $\epsilon_\mathrm{t} = 0$ denotes the total loss of tangential relative velocity after the impact, while $\epsilon_\mathrm{t} \in [+1, -1]$ describe two elastic limits, i.e smooth and rough particles, respectively, [17]. Smooth particles are represented by $\epsilon_\mathrm{t} = 1$ as the tangential relative velocity and thus the angular relative velocity of the interacting particles is not changed during the collision, [18]. Rough particles are represented by $\epsilon_\mathrm{t} = -1$, which leads to a reversal of the tangential relative velocities at impact, [18]. Becker et al. [18], described this case as (in 2D) very elastic gear wheels. In the following, we base our derivation of the tangential restitution coefficient on the Coulomb friction model, effectively reducing the range of ϵ_t to $0 \le \epsilon_\mathrm{t} \le 1$. Note that there are various alternative contact force laws available in the literature, see [45–47].

3. Conservation equations during collision

In the following, we will present the momentum conservation equations during collision of particles. The conservation of linear momentum is given by:

$$m_1\boldsymbol{v}_1 + m_2\boldsymbol{v}_2 = m_1\boldsymbol{c}_1 + m_2\boldsymbol{c}_2\,, \tag{8}$$

where the particle velocity before and after the impact are denoted as $\boldsymbol{v}_\varphi$ and $\boldsymbol{c}_\varphi$ ($\varphi = 1, 2$), respectively. The particle velocity at the contact point is obtained as follows

$$\boldsymbol{v}_{\mathrm{P},\varphi} = \boldsymbol{v}_\varphi - \boldsymbol{\omega}_\varphi \times \boldsymbol{r}^*_\varphi, \qquad \boldsymbol{c}_{\mathrm{P},\varphi} = \boldsymbol{c}_\varphi - \boldsymbol{\psi}_\varphi \times \boldsymbol{r}^*_\varphi\,, \tag{9}$$

where the pre- and post-collisional angular velocities are labeled as $\boldsymbol{\omega}_\varphi$ and $\boldsymbol{\psi}_\varphi$, respectively. Recall that $\boldsymbol{r}^*_\varphi$ denotes the distance vector pointing from the collision point to the respective particle center, see Fig. 1, thus explaining the negative sign of the terms $\boldsymbol{\omega}_\varphi \times \boldsymbol{r}^*_\varphi$. From Eq. (6) the pre- and post-collision point normal relative velocities $\boldsymbol{v}^\mathrm{n}_{\mathrm{P},21}$ and $\boldsymbol{c}^\mathrm{n}_{\mathrm{P},21}$, respectively, are related through the normal restitution coefficient as follows:

$$\underbrace{\boldsymbol{e}_\mathrm{n}\cdot\left[\boldsymbol{c}_{\mathrm{P},2} - \boldsymbol{c}_{\mathrm{P},1}\right]}_{c^\mathrm{n}_{\mathrm{P},21}} = -\epsilon_\mathrm{n}\underbrace{\boldsymbol{e}_\mathrm{n}\cdot\left[\boldsymbol{v}_{\mathrm{P},2} - \boldsymbol{v}_{\mathrm{P},1}\right]}_{v^\mathrm{n}_{\mathrm{P},21}}. \tag{10}$$

Likewise from Eq. (7), the pre- and post-collision tangential relative velocities are related by:

$$\underbrace{\boldsymbol{e}_\mathrm{t}\cdot\left[\boldsymbol{c}_{\mathrm{P},2} - \boldsymbol{c}_{\mathrm{P},1}\right]}_{c^\mathrm{t}_{\mathrm{P},21}} = +\epsilon_\mathrm{t}\underbrace{\boldsymbol{e}_\mathrm{t}\cdot\left[\boldsymbol{v}_{\mathrm{P},2} - \boldsymbol{v}_{\mathrm{P},1}\right]}_{v^\mathrm{t}_{\mathrm{P},21}}. \tag{11}$$

The cFoR $\boldsymbol{e}''_x$ unit vector is aligned with the collision normal $\boldsymbol{e}_\mathrm{n}$ with corresponding coefficient matrix $\underline{e}''_\mathrm{n} = [1,\ 0,\ 0]^\mathrm{T}$. Likewise the unit vector $\boldsymbol{e}''_y$ is aligned with the tangential relative velocity in the contact point and thus with $\boldsymbol{e}_\mathrm{t}$ with corresponding coefficient matrix $\underline{e}''_\mathrm{t} = [0,\ 1,\ 0]^\mathrm{T}$. Thus, we can simplify Eqs. (10)–(11) to:

$$\begin{aligned} &c''_{x,2} + r''_{y,2}\psi''_{z,2} - r''_{z,2}\psi''_{y,2} - c''_{x,1} - r''_{1y}\psi''_{z,1} + r''_{z,1}\psi''_{1y} = \\ &-\epsilon_\mathrm{n}\left[v''_{x,2} + r''_{y,2}\omega''_{z,2} - r''_{z,2}\omega''_{y,2} - v''_{x,1} - r''_{y,1}\omega''_{z,1} + r''_{z,1}\omega''_{y,1}\right] \end{aligned} \tag{12}$$

and

$$\begin{aligned} &c''_{y,2} - r''_{x,2}\psi''_{z,2} + r''_{z,2}\psi''_{x,2} - c''_{y,1} + r''_{x,1}\psi''_{z,1} - r''_{z,1}\psi''_{x,1} = \\ &+\epsilon_\mathrm{t}\left[v''_{y,2} - r''_{x,2}\omega''_{z,2} + r''_{z,2}\omega''_{x,2} - v''_{y,1} + r''_{x,1}\omega''_{z,1} - r''_{z,1}\omega''_{x,1}\right]. \end{aligned} \tag{13}$$

With respect to the collision point, the conservation of angular momentum can be expressed for each particle separately as

$$\boldsymbol{I}_\varphi\cdot\boldsymbol{\omega}_\varphi + \boldsymbol{r}^*_\varphi \times m_\varphi\boldsymbol{v}_\varphi = \boldsymbol{I}_\varphi\cdot\boldsymbol{\psi}_\varphi + \boldsymbol{r}^*_\varphi \times m_\varphi\boldsymbol{c}_\varphi\,, \tag{14}$$

rendering the expression for the post-collision angular velocities

$$\boldsymbol{\psi}_\varphi = \boldsymbol{\omega}_\varphi + \underbrace{\boldsymbol{I}^{-1}_\varphi\cdot\left[\boldsymbol{r}^*_\varphi \times m_\varphi\left[\boldsymbol{v}_\varphi - \boldsymbol{c}_\varphi\right]\right]}_{\Delta\boldsymbol{\omega}_\varphi}. \tag{15}$$

This representation is valid since here the reference point for the balance of angular momentum is chosen as the contact point, thus the contact force does not contribute to the angular momentum.[1]

Eventually, combining the results of linear and angular momentum, we can set up a linear system of equations in the format $\underline{A}\,\underline{x} = \underline{b}$ and solve for the ten unknowns:

$$\underline{x} = \left[\ c''_{x,1},\ c''_{y,1},\ c''_{x,2},\ c''_{y,2},\ \psi''_{x,1},\ \psi''_{y,1},\ \psi''_{z,1},\ \psi''_{x,2},\ \psi''_{y,2},\ \psi''_{z,2}\ \right]^\mathrm{T}. \tag{16}$$

(Note that $c''_{z,\varphi} = v''_{z,\varphi}$ are known beforehand). To this end, we use Eq. (8), which gives us two non-zero equations in the collision frame, together with Eqs. (12) and (13), which give us two further equations, and finally Eq. (14) gives us the missing six equations as it can be written for each particle separately.

4. Derivation of an expression for the tangential restitution coefficient ϵ_t

4.1. Change of linear momentum

From the conservation of linear momentum in Eq. (8), we define the change of linear momentum $\Delta\boldsymbol{p}$ as

$$\Delta\boldsymbol{p} = \underbrace{m_1\left[\boldsymbol{c}_1 - \boldsymbol{v}_1\right]}_{\Delta\boldsymbol{p}_1} = \underbrace{-m_2\left[\boldsymbol{c}_2 - \boldsymbol{v}_2\right]}_{-\Delta\boldsymbol{p}_2}, \tag{17}$$

which allows the representations

$$\boldsymbol{c}_1 = +\frac{\Delta\boldsymbol{p}}{m_1} + \boldsymbol{v}_1\,, \qquad \boldsymbol{c}_2 = -\frac{\Delta\boldsymbol{p}}{m_2} + \boldsymbol{v}_2\,. \tag{18}$$

The change of linear momentum can be decomposed into normal and tangential contributions:

$$\Delta\boldsymbol{p} = \Delta\boldsymbol{p}^\mathrm{n} + \Delta\boldsymbol{p}^\mathrm{t} = \underbrace{\left[\Delta\boldsymbol{p}^\mathrm{n}\cdot\boldsymbol{e}^\mathrm{n}\right]}_{\Delta p^\mathrm{n}}\boldsymbol{e}^\mathrm{n} + \underbrace{\left[\Delta\boldsymbol{p}^\mathrm{t}\cdot\boldsymbol{e}^\mathrm{t}\right]}_{\Delta p^\mathrm{t}}\boldsymbol{e}^\mathrm{t}\,. \tag{19}$$

Observe, that due to the definition of $\boldsymbol{e}^\mathrm{n}$ and $\boldsymbol{e}^\mathrm{t}$, see Fig. 1, $\Delta p^\mathrm{n} \ge 0$, whereas Δp^t can take arbitrary values.

[1] The conservation of angular momentum for a particle φ with respect to an arbitrary reference point A can be written as follows: $\boldsymbol{I}_\varphi\cdot\left[\boldsymbol{\omega}_\varphi - \boldsymbol{\psi}_\varphi\right] + m_\varphi\boldsymbol{r}_\varphi \times \left[\boldsymbol{v}_\varphi - \boldsymbol{c}_\varphi\right] = \boldsymbol{r}_{\mathrm{P},\varphi} \times \boldsymbol{F}$, $\varphi = 1, 2$. The impulse moment is expanded as $\boldsymbol{r}_{\mathrm{P},\varphi} \times \boldsymbol{F} = \left[\boldsymbol{r}_\varphi - \boldsymbol{r}^*_\varphi\right] \times \boldsymbol{F}$. Note that $\boldsymbol{r}_\mathrm{P}$ points from the reference point A to the contact point P, $\boldsymbol{r}_\varphi$ points from the reference point A to the particle center, while $\boldsymbol{r}^*_\varphi$ points from P to the particle center, see Fig. 1. If the contact point P is identical to the reference point A, we obtain $\boldsymbol{r}_\varphi = \boldsymbol{r}^*_\varphi$, thus $\boldsymbol{r}_{\mathrm{P},\varphi} = \boldsymbol{0}$ and consequently $\boldsymbol{r}_{\mathrm{P},\varphi} \times \boldsymbol{F} = \boldsymbol{0}$.

4.2. Change of linear momentum in normal direction

The change of normal linear momentum $\Delta \boldsymbol{p}^{\mathrm{n}}$ is expressed using the respective normal velocities

$$\Delta \boldsymbol{p}^{\mathrm{n}} = \underbrace{m_1 \left[\boldsymbol{c}_1^{\mathrm{n}} - \boldsymbol{v}_1^{\mathrm{n}}\right]}_{\Delta \boldsymbol{p}_1^{\mathrm{n}}} = \underbrace{-m_2 \left[\boldsymbol{c}_2^{\mathrm{n}} - \boldsymbol{v}_2^{\mathrm{n}}\right]}_{-\Delta \boldsymbol{p}_2^{\mathrm{n}}}, \tag{20}$$

whereby we detail corresponding to Eq. (18)

$$\boldsymbol{c}_1^{\mathrm{n}} = +\frac{\Delta \boldsymbol{p}^{\mathrm{n}}}{m_1} + \boldsymbol{v}_1^{\mathrm{n}}, \qquad \boldsymbol{c}_2^{\mathrm{n}} = -\frac{\Delta \boldsymbol{p}^{\mathrm{n}}}{m_2} + \boldsymbol{v}_2^{\mathrm{n}}. \tag{21}$$

Next, the aim is to find an expression for the unknown post-collision normal velocities $\boldsymbol{c}_{\mathrm{P},\varphi}^{\mathrm{n}}$ in the contact point P. Note that using Eq. (9) we write

$$\boldsymbol{c}_{\mathrm{P},2}^{\mathrm{n}} = \left[\boldsymbol{c}_{\mathrm{P},2} \cdot \boldsymbol{e}_{\mathrm{n}}\right] \boldsymbol{e}_{\mathrm{n}} = \left[\left[\boldsymbol{c}_2 - \boldsymbol{\psi}_2 \times \boldsymbol{r}_2^*\right] \cdot \boldsymbol{e}_{\mathrm{n}}\right] \boldsymbol{e}_{\mathrm{n}} = \boldsymbol{c}_2^{\mathrm{n}} - \left[\left[\boldsymbol{\psi}_2 \times \boldsymbol{r}_2^*\right] \cdot \boldsymbol{e}_{\mathrm{n}}\right] \boldsymbol{e}_{\mathrm{n}}. \tag{22}$$

Now we insert the expression for $\boldsymbol{c}_2^{\mathrm{n}}$ from Eq. (21) into Eq. (22), whereby we identify that $\boldsymbol{v}_2^{\mathrm{n}} = \boldsymbol{v}_{\mathrm{P},2}^{\mathrm{n}} + \left[\left[\boldsymbol{\omega}_2 \times \boldsymbol{r}_2^*\right] \cdot \boldsymbol{e}^{\mathrm{n}}\right] \boldsymbol{e}^{\mathrm{n}}$ which renders

$$\boldsymbol{c}_{\mathrm{P},2}^{\mathrm{n}} = -\frac{\Delta \boldsymbol{p}^{\mathrm{n}}}{m_2} + \boldsymbol{v}_{\mathrm{P},2}^{\mathrm{n}} + \left[\left[\boldsymbol{\omega}_2 \times \boldsymbol{r}_2^* - \boldsymbol{\psi}_2 \times \boldsymbol{r}_2^*\right] \cdot \boldsymbol{e}_{\mathrm{n}}\right] \boldsymbol{e}_{\mathrm{n}}. \tag{23}$$

Furthermore, we can express $\boldsymbol{\psi}_{\varphi}$ by Eq. (15), where we recall the definition of $\Delta \boldsymbol{p}$, see Eq. (17)

$$\boldsymbol{\psi}_2 = \boldsymbol{\omega}_2 + \Delta \boldsymbol{\omega}_2 \quad \text{with} \quad \Delta \boldsymbol{\omega}_2 = +\boldsymbol{I}_2^{-1} \cdot \left[\boldsymbol{r}_2^* \times \Delta \boldsymbol{p}\right], \tag{24}$$

$$\boldsymbol{\psi}_1 = \boldsymbol{\omega}_1 + \Delta \boldsymbol{\omega}_1 \quad \text{with} \quad \Delta \boldsymbol{\omega}_1 = -\boldsymbol{I}_1^{-1} \cdot \left[\boldsymbol{r}_1^* \times \Delta \boldsymbol{p}\right]. \tag{25}$$

Inserting Eq. (24) into Eq. (23) thus renders

$$\boldsymbol{c}_{\mathrm{P},2}^{\mathrm{n}} = -\frac{\Delta \boldsymbol{p}^{\mathrm{n}}}{m_2} + \boldsymbol{v}_{\mathrm{P},2}^{\mathrm{n}} - \left[\left[\Delta \boldsymbol{\omega}_2 \times \boldsymbol{r}_2^*\right] \cdot \boldsymbol{e}_{\mathrm{n}}\right] \boldsymbol{e}_{\mathrm{n}}. \tag{26}$$

In a similar fashion, we obtain the expression for $\boldsymbol{c}_{\mathrm{P},1}^{\mathrm{n}}$

$$\boldsymbol{c}_{\mathrm{P},1}^{\mathrm{n}} = +\frac{\Delta \boldsymbol{p}^{\mathrm{n}}}{m_1} + \boldsymbol{v}_{\mathrm{P},1}^{\mathrm{n}} - \left[\left[\Delta \boldsymbol{\omega}_1 \times \boldsymbol{r}_1^*\right] \cdot \boldsymbol{e}_{\mathrm{n}}\right] \boldsymbol{e}_{\mathrm{n}}. \tag{27}$$

Finally, we insert $\boldsymbol{c}_{\mathrm{P},2}^{\mathrm{n}}$ (Eq. (26)) and $\boldsymbol{c}_{\mathrm{P},1}^{\mathrm{n}}$ (Eq. (27)) into the vectorial version of Eq. (6), which can be rewritten as

$$\Delta \boldsymbol{p}^{\mathrm{n}} = m_{\mathrm{eff}} \boldsymbol{v}_{\mathrm{P},21}^{\mathrm{n}} \left[1 + \epsilon_{\mathrm{n}}\right] - m_{\mathrm{eff}} \left[\left[\Delta \boldsymbol{\omega}_2 \times \boldsymbol{r}_2^* - \Delta \boldsymbol{\omega}_1 \times \boldsymbol{r}_1^*\right] \cdot \boldsymbol{e}_{\mathrm{n}}\right] \boldsymbol{e}_{\mathrm{n}}, \tag{28}$$

where the effective mass is abbreviated as $m_{\mathrm{eff}} = m_1 m_2 / \left[m_1 + m_2\right]$. Eq. (28) presents a useful relation between the change of normal linear momentum and the normal restitution coefficient ϵ_{n}.

4.3. Change of linear momentum in tangential direction

To derive an expression for the tangential restitution coefficient ϵ_{t}, we need to replace $\boldsymbol{c}_{\mathrm{P},1}^{\mathrm{t}}$ and $\boldsymbol{c}_{\mathrm{P},2}^{\mathrm{t}}$ in the vectorial version of Eq. (7). Note that we can obtain the post-collisional tangential velocities in the collision point from the collision point velocity $\boldsymbol{c}_{\mathrm{P},\varphi}$ (Eq. (9)) and the normal collision point velocity $\boldsymbol{c}_{\mathrm{P},\varphi}^{\mathrm{n}}$:

$$\boldsymbol{c}_{\mathrm{P},\varphi}^{\mathrm{t}} = \boldsymbol{c}_{\mathrm{P},\varphi} - \boldsymbol{c}_{\mathrm{P},\varphi}^{\mathrm{n}} = \boldsymbol{c}_{\varphi} - \boldsymbol{\psi}_{\varphi} \times \boldsymbol{r}_{\varphi}^* - \boldsymbol{c}_{\mathrm{P},\varphi}^{\mathrm{n}}. \tag{29}$$

Inserting Eq. (29) into the vectorial version of Eq. (7), we obtain:

$$\boldsymbol{c}_2 - \boldsymbol{\psi}_2 \times \boldsymbol{r}_2^* - \boldsymbol{c}_{\mathrm{P},2}^{\mathrm{n}} - \boldsymbol{c}_1 + \boldsymbol{\psi}_1 \times \boldsymbol{r}_1^* + \boldsymbol{c}_{\mathrm{P},1}^{\mathrm{n}} = \epsilon_{\mathrm{t}} \boldsymbol{v}_{\mathrm{P},21}^{\mathrm{t}}. \tag{30}$$

Inserting the expressions for $\boldsymbol{c}_{\varphi}$ (Eq. (18)) and $\boldsymbol{c}_{\mathrm{P},\varphi}^{\mathrm{n}}$ (Eq. (22)), we write

$$-\frac{\Delta \boldsymbol{p}^{\mathrm{t}}}{m_{\mathrm{eff}}} + \boldsymbol{v}_2 - \boldsymbol{v}_2^{\mathrm{n}} - \boldsymbol{v}_1 + \boldsymbol{v}_1^{\mathrm{n}} - \left[\left[\boldsymbol{\psi}_2 \times \boldsymbol{r}_2^*\right] \cdot \boldsymbol{e}_{\mathrm{t}}\right] \boldsymbol{e}_{\mathrm{t}} + \left[\left[\boldsymbol{\psi}_1 \times \boldsymbol{r}_1^*\right] \cdot \boldsymbol{e}_{\mathrm{t}}\right] \boldsymbol{e}_{\mathrm{t}}, \tag{31}$$

where we used $\left[\left[\boldsymbol{\psi}_{\varphi} \times \boldsymbol{r}_{\varphi}^*\right] \cdot \boldsymbol{e}_{\mathrm{n}}\right] \boldsymbol{e}_{\mathrm{n}} - \boldsymbol{\psi}_{\varphi} \times \boldsymbol{r}_{\varphi}^* = -\left[\left[\boldsymbol{\psi}_{\varphi} \times \boldsymbol{r}_{\varphi}^*\right] \cdot \boldsymbol{e}_{\mathrm{t}}\right] \boldsymbol{e}_{\mathrm{t}}$. Furthermore, we use

$$\boldsymbol{v}_2 - \boldsymbol{v}_2^{\mathrm{n}} - \boldsymbol{v}_1 + \boldsymbol{v}_1^{\mathrm{n}} = \boldsymbol{v}_2^{\mathrm{t}} - \boldsymbol{v}_1^{\mathrm{t}} = \boldsymbol{v}_{\mathrm{P},2}^{\mathrm{t}} + \left[\left[\boldsymbol{\omega}_2 \times \boldsymbol{r}_2^*\right] \cdot \boldsymbol{e}_{\mathrm{t}}\right] \boldsymbol{e}_{\mathrm{t}} - \left[\boldsymbol{v}_{\mathrm{P},1}^{\mathrm{t}} + \left[\boldsymbol{\omega}_1 \times \boldsymbol{r}_1^*\right] \cdot \boldsymbol{e}_{\mathrm{t}}\right] \boldsymbol{e}_{\mathrm{t}} \tag{32}$$

and finally insert the expressions for $\boldsymbol{\psi}_1$ and $\boldsymbol{\psi}_2$ (Eq. (24)), to obtain

$$\Delta \boldsymbol{p}^{\mathrm{t}} = m_{\mathrm{eff}} \boldsymbol{v}_{\mathrm{P},21}^{\mathrm{t}} \left[1 - \epsilon_{\mathrm{t}}\right] - m_{\mathrm{eff}} \left[\left[\Delta \boldsymbol{\omega}_2 \times \boldsymbol{r}_2^* - \Delta \boldsymbol{\omega}_1 \times \boldsymbol{r}_1^*\right] \cdot \boldsymbol{e}_{\mathrm{t}}\right] \boldsymbol{e}_{\mathrm{t}}. \tag{33}$$

Eq. (33) presents a useful relation between the change of tangential linear momentum and the tangential restitution coefficient ϵ_{t}.

Note the formal similarities of Eqs. (28) and (33) with a pertinent change of sign for the respective restitution coefficient.

4.4. Constitutive law

To express the change of the normal and tangential linear momentum ($\Delta \boldsymbol{p}^{\mathrm{n}}$, $\Delta \boldsymbol{p}^{\mathrm{t}}$), we employ a constitutive law. Note that the impulses can be obtained in terms of the contact forces

$$\Delta \boldsymbol{p}^{\mathrm{n}} \equiv \Delta \boldsymbol{p}_1^{\mathrm{n}} = +\int_{t_1}^{t_2} \boldsymbol{F}_1^{\mathrm{n}} dt, \qquad \Delta \boldsymbol{p}_2^{\mathrm{n}} = -\int_{t_1}^{t_2} \boldsymbol{F}_1^{\mathrm{n}} dt = -\Delta \boldsymbol{p}^{\mathrm{n}}, \tag{34}$$

and

$$\Delta \boldsymbol{p}^{\mathrm{t}} \equiv \Delta \boldsymbol{p}_1^{\mathrm{t}} = +\int_{t_1}^{t_2} \boldsymbol{F}_1^{\mathrm{t}} dt, \qquad \Delta \boldsymbol{p}_2^{\mathrm{t}} = -\int_{t_1}^{t_2} \boldsymbol{F}_1^{\mathrm{t}} dt = -\Delta \boldsymbol{p}^{\mathrm{t}}. \tag{35}$$

In the following, we assume Coulomb friction. Thus, we assume that during the entire impact the particles slide, [17]:

$$\boldsymbol{F}_1^{\mathrm{t}} = -\mathrm{sgn}(v_{\mathrm{P},12}^{\mathrm{t}}) \mu |\boldsymbol{F}_1^{\mathrm{n}}| \boldsymbol{e}_{\mathrm{t}} = \mathrm{sgn}(v_{\mathrm{P},21}^{\mathrm{t}}) \mu |\boldsymbol{F}_1^{\mathrm{n}}| \boldsymbol{e}_{\mathrm{t}}. \tag{36}$$

Note that $\boldsymbol{e}_{\mathrm{t}}$ is defined to point in the direction of relative tangential velocity of the collision point $v_{\mathrm{P},21}^{\mathrm{t}}$, thus $-\mathrm{sgn}(v_{\mathrm{P},12}^{\mathrm{t}}) = \mathrm{sgn}(v_{\mathrm{P},21}^{\mathrm{t}}) = 1$. Consequently, we can rewrite the tangential impulse as

$$\Delta \boldsymbol{p}^{\mathrm{t}} = \int_{t_1}^{t_2} \mu |\boldsymbol{F}_1^{\mathrm{n}}| \boldsymbol{e}_{\mathrm{t}} dt = \mu \int_{t_1}^{t_2} |\boldsymbol{F}_1^{\mathrm{n}}| \, dt \, \boldsymbol{e}_{\mathrm{t}} = \mu |\Delta \boldsymbol{p}^{\mathrm{n}}| \boldsymbol{e}_{\mathrm{t}} = \mu \Delta p^{\mathrm{n}} \boldsymbol{e}_{\mathrm{t}}. \tag{37}$$

Recall that we assume that $\boldsymbol{e}_{\mathrm{n}}$ points in the direction of the change of normal momentum and thus $\Delta \boldsymbol{p}^{\mathrm{n}} = \left[\Delta \boldsymbol{p}^{\mathrm{n}} \cdot \boldsymbol{e}_{\mathrm{n}}\right] \boldsymbol{e}_{\mathrm{n}} = \Delta p^{\mathrm{n}} \boldsymbol{e}_{\mathrm{n}}$ with $\Delta p^{\mathrm{n}} \geq 0$ and $\Delta \boldsymbol{p} = \Delta p^{\mathrm{n}} \boldsymbol{e}_{\mathrm{n}} + \Delta \boldsymbol{p}^{\mathrm{t}}$.

Now we insert the constitutive expression for $\Delta \boldsymbol{p}^{\mathrm{t}}$ (Eq. (37)) into the expressions for $\Delta \boldsymbol{\omega}_{\varphi}$, see Eqs. (24)–(25) and obtain

$$\Delta \boldsymbol{\omega}_2 = +\Delta p^n \boldsymbol{I}_2^{-1} \cdot \left[\boldsymbol{r}_2^* \times \left[\boldsymbol{e}_{\mathrm{n}} + \mu \boldsymbol{e}_{\mathrm{t}}\right]\right], \tag{38}$$

$$\Delta \boldsymbol{\omega}_1 = -\Delta p^n \boldsymbol{I}_1^{-1} \cdot \left[\boldsymbol{r}_1^* \times \left[\boldsymbol{e}_{\mathrm{n}} + \mu \boldsymbol{e}_{\mathrm{t}}\right]\right]. \tag{39}$$

Next, we use the above equations in Eq. (28), which is first rewritten as

$$\Delta \boldsymbol{p}^{\mathrm{n}} = m_{\mathrm{eff}} \boldsymbol{v}_{\mathrm{P},21}^{\mathrm{n}} \left[\epsilon_{\mathrm{n}} + 1\right] - m_{\mathrm{eff}} \left[\left[\Delta \tilde{\boldsymbol{\omega}}_2 \times \boldsymbol{r}_2^* - \Delta \tilde{\boldsymbol{\omega}}_1 \times \boldsymbol{r}_1^*\right] \cdot \boldsymbol{e}_{\mathrm{n}}\right] \Delta \boldsymbol{p}^{\mathrm{n}} \tag{40}$$

using the normalization $\Delta \tilde{\boldsymbol{\omega}}_{\varphi} = \Delta \boldsymbol{\omega}_{\varphi} / \Delta p^{\mathrm{n}}$. Note that $\Delta \tilde{\boldsymbol{\omega}}_{\varphi}$ are computable from Eqs. (38)–(39). Next, we can regroup terms in Eq. (40) as

$$\Delta \boldsymbol{p}^{\mathrm{n}} \left[1 + \underbrace{m_{\mathrm{eff}} \left[\Delta \tilde{\boldsymbol{\omega}}_2 \times \boldsymbol{r}_2^* - \Delta \tilde{\boldsymbol{\omega}}_1 \times \boldsymbol{r}_1^*\right] \cdot \boldsymbol{e}_{\mathrm{n}}}_{\gamma}\right] = m_{\mathrm{eff}} \boldsymbol{v}_{\mathrm{P},21}^{\mathrm{n}} \left[\epsilon_{\mathrm{n}} + 1\right], \tag{41}$$

which, with the definition of γ as

$$\gamma = m_{\mathrm{eff}} \left[\Delta \tilde{\boldsymbol{\omega}}_2 \times \boldsymbol{r}_2^* - \Delta \tilde{\boldsymbol{\omega}}_1 \times \boldsymbol{r}_1^*\right] \cdot \boldsymbol{e}_{\mathrm{n}}, \tag{42}$$

can be further simplified to

$$\Delta \boldsymbol{p}^{\mathrm{n}} = m_{\mathrm{eff}} \boldsymbol{v}_{\mathrm{P},21}^{\mathrm{n}} \left[\epsilon_{\mathrm{n}} + 1\right] \left[1 + \gamma\right]^{-1}. \tag{43}$$

Finally, to obtain the expression for ϵ_{t} we insert the law for $\Delta \boldsymbol{p}^{\mathrm{t}}$ (Eq. (37)), into Eq. (33) and obtain

$$\mu \Delta p^{\mathrm{n}} \boldsymbol{e}_{\mathrm{t}} = m_{\mathrm{eff}} \boldsymbol{v}_{\mathrm{P},21}^{\mathrm{t}} \left[1 - \epsilon_{\mathrm{t}}\right] - \beta \Delta p^{\mathrm{n}} \boldsymbol{e}_{\mathrm{t}}, \tag{44}$$

with β defined as

$$\beta = m_{\mathrm{eff}} \left[\Delta \tilde{\boldsymbol{\omega}}_2 \times \boldsymbol{r}_2^* - \Delta \tilde{\boldsymbol{\omega}}_1 \times \boldsymbol{r}_1^*\right] \cdot \boldsymbol{e}_{\mathrm{t}}. \tag{45}$$

By regrouping, Eq. (44) simplifies to

$$\Delta p^{\mathrm{n}} \left[\mu + \beta\right] \boldsymbol{e}_{\mathrm{t}} = m_{\mathrm{eff}} \boldsymbol{v}_{\mathrm{P},21}^{\mathrm{t}} \left[1 - \epsilon_{\mathrm{t}}\right]. \tag{46}$$

Next we insert the normal projection of $\Delta \boldsymbol{p}^{\mathrm{n}}$ from Eq. (43) for $\Delta \boldsymbol{p}^{\mathrm{n}}$ and obtain

$$\epsilon_{\mathrm{t}} \boldsymbol{v}_{\mathrm{P},21}^{\mathrm{t}} = \boldsymbol{v}_{\mathrm{P},21}^{\mathrm{t}} - \left[v_{\mathrm{P},21}^{\mathrm{n}} \left[\epsilon_{\mathrm{n}} + 1\right] \left[1+\gamma\right]^{-1} \right] \left[\mu + \beta\right] \boldsymbol{e}_{\mathrm{t}} \,. \tag{47}$$

Eventually, by projecting Eq. (47) to the tangential direction $\boldsymbol{e}_{\mathrm{t}}$, we obtain the final expression for the tangential restitution coefficient ϵ_{t} for arbitrarily shaped particles under the assumption of Coulomb friction

$$\boxed{\epsilon_{\mathrm{t}} = 1 - \frac{\epsilon_{\mathrm{n}} + 1}{1+\gamma} \left[\mu + \beta\right] \frac{v_{\mathrm{P},21}^{\mathrm{n}}}{v_{\mathrm{P},21}^{\mathrm{t}}} \,.} \tag{48}$$

As an important consequence, we find that the coefficient of tangential restitution does significantly depend on both the normal and the tangential relative velocities. In case of vanishing relative normal velocity $v_{\mathrm{P},21}^{\mathrm{n}} \to 0$, we observe that for all particle shapes $\epsilon_{\mathrm{t}} \to 1$. However, in the case of $v_{\mathrm{P},21}^{\mathrm{n}} \gg v_{\mathrm{P},21}^{\mathrm{t}}$, we obtain for all particle shapes $\epsilon_t \to 0$, if we set the minimum of the tangential restitution coefficient to $\epsilon_{\mathrm{t,min}} = 0$, as employed by Schwager et al. [17].

4.5. Validation for spheres

We validate the expression Eq. (48) for the case of spherical particles. Note that for spherical particles $\gamma_{\mathrm{sph}} = 0$ since $\left[\Delta\tilde{\boldsymbol{\omega}}_{\varphi} \times \boldsymbol{r}_{\varphi}^{*}\right] \cdot \boldsymbol{e}_{\mathrm{n}} = 0$. Furthermore, we can obtain β_{sph} using the following reduced expressions for $\Delta\tilde{\boldsymbol{\omega}}_{\varphi}$

$$\Delta\tilde{\boldsymbol{\omega}}_2 = +\boldsymbol{I}_2^{-1} \cdot \left[\boldsymbol{r}_2^{*} \times \mu \boldsymbol{e}_{\mathrm{t}}\right] \,, \tag{49}$$

$$\Delta\tilde{\boldsymbol{\omega}}_1 = -\boldsymbol{I}_1^{-1} \cdot \left[\boldsymbol{r}_1^{*} \times \mu \boldsymbol{e}_{\mathrm{t}}\right] \,, \tag{50}$$

since $\boldsymbol{r}_{\varphi}^{*} \times \boldsymbol{e}_{\mathrm{n}} = \boldsymbol{0}$, the sphericity of $\boldsymbol{I}_{\varphi} \propto I_{\varphi}$, and $\left[\boldsymbol{r}_{\varphi}^{*} \times \boldsymbol{e}_{\mathrm{t}}\right] \times \boldsymbol{r}_{\varphi}^{*} = r_{\varphi}^{*2} \boldsymbol{e}_{\mathrm{t}}$ (as $\boldsymbol{r}_{\varphi}^{*} \cdot \boldsymbol{e}_{\mathrm{t}} = 0$). Followingly, we can write

$$\begin{aligned} \beta_{\mathrm{sph}} &= m_{\mathrm{eff}} \left[\left[\boldsymbol{I}_2^{-1} \cdot \left[\boldsymbol{r}_2^{*} \times \mu \boldsymbol{e}_{\mathrm{t}}\right] \times \boldsymbol{r}_2^{*} + \boldsymbol{I}_1^{-1} \cdot \left[\boldsymbol{r}_1^{*} \times \mu \boldsymbol{e}_{\mathrm{t}}\right] \times \boldsymbol{r}_1^{*}\right] \cdot \boldsymbol{e}_{\mathrm{t}} \right] \\ &= \mu m_{\mathrm{eff}} \left[I_2^{-1} r_2^{*2} + I_1^{-1} r_1^{*2} \right] \,. \end{aligned} \tag{51}$$

Consequently, we obtain for Eq. (48)

$$\epsilon_{\mathrm{t,sph}} = 1 - \frac{\mu \left[\epsilon_{\mathrm{n}} + 1\right]}{\alpha^{-1}} \frac{v_{\mathrm{P},12}^{\mathrm{n}}}{v_{\mathrm{P},12}^{\mathrm{t}}} \,, \tag{52}$$

with α defined as

$$\alpha = \left[1 + m_{\mathrm{eff}} \left[I_2^{-1} r_2^2 + I_1^{-1} r_1^2\right]\right] \,, \tag{53}$$

which is in agreement with the tangential restitution coefficient presented in [17,18].

5. Demonstrative examples

We investigate the dependency of the tangential restitution coefficient ϵ_{t} on the normal ($v_{\mathrm{P},21}^{\mathrm{n}}$) and tangential ($v_{\mathrm{P},21}^{\mathrm{t}}$) relative velocities, the aspect ratios λ_1, λ_2 as well as the shape factors s_1, s_2 in the case of Coulomb friction. In this context, we employ demonstrative examples of particle-collisions of prolate, oblate as well as diamond and cubic-like particles.

5.1. Collision configuration I

To study the novel tangential restitution model for arbitrary particles, we select specific collision configurations. As a first step, we compare head-on particle collisions as displayed in Fig. 2 for spherical as well as superellipsoidal particles. Note that in this example, normal velocities are present in $\boldsymbol{e}_1$ direction, whereas $\boldsymbol{e}_2$ is aligned with the tangential relative velocity $v_{\mathrm{P},21}^{\mathrm{t}}$. Becker et al. [18] studied the coefficient of tangential restitution for steel particles of perfect spherical shape ($\alpha = 7/2$) as a function of the components of the normal and tangential impact velocities in the case of Coulomb friction. To match the results

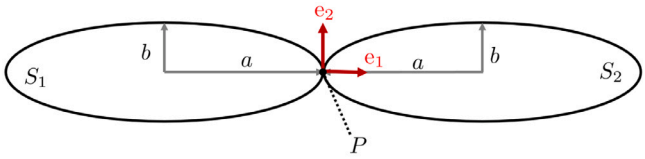

Fig. 2. Sketch of head-on particle collision of two prolate particles (S_1, S_2) with half-axis a, b, b ($= c$), including collision frame $\boldsymbol{e}_1$, $\boldsymbol{e}_2$ and contact point P_{coll}.

of Becker et al. [18], we employ identical material parameters: $\mu = 0.4$, $d_{eq} = 0.04\,\mathrm{m}$, $\rho_p = 7850\,\mathrm{kg/m^3}$, $\epsilon_{\mathrm{n}} = 1$ in all the following simulations.

In case of the centric head-on collision of two identical particles and $v_{\mathrm{P},21}^{\mathrm{n}} > 0$, Eq. (48) simplifies to

$$\epsilon_{\mathrm{t}} = 1 - \mu \left[\epsilon_{\mathrm{n}} + 1\right] \underbrace{\left[1 + m_{\mathrm{eff}} \left[2 I_{zz}^{-1} r_x^2\right]\right]}_{\alpha} \frac{v_{\mathrm{P},21}^{\mathrm{n}}}{v_{\mathrm{P},21}^{\mathrm{t}}} \tag{54}$$

as for two identical particles in collision $I_{zz} = I_{zz,1} = I_{zz,2}$ and $r_x^2 = r_{x,1}^2 = r_{x,2}^2$.

5.1.1. Spherical particles

For spherical particles of equal mass and radius, the term α in Eq. (53) simplifies to 7/2 since $I_{zz} = 2/5\ ma^2$, $r_x^2 = a^2$, and $m_{\mathrm{eff}} = m/2$ for all collision configurations. For spherical particles, we obtain Fig. 3(a), which shows the dependence of the tangential restitution coefficient ϵ_{t} on the normal and tangential relative particle velocities. As shown, our novel model, as described in Eq. (47), gives identical results to the model used by Schwager et al. [17] for Coulomb friction. In Fig. 3 (a,b), the general trend is observed that ϵ_{t} increases with increasing $v_{\mathrm{P},21}^{\mathrm{t}}$ and ϵ_{t} decreases with increasing $v_{\mathrm{P},21}^{\mathrm{n}}$. As indicated in Eq. (48), we observe in Fig. 3 (a) that for $v_{\mathrm{P},21}^{\mathrm{n}} = 0$ we obtain $\epsilon_{\mathrm{t}} = 1$, leading to a conservation of the tangential relative particle velocity during the collision. Moreover, for $v_{\mathrm{P},21}^{\mathrm{n}} > 0$ we obtain $\epsilon_{\mathrm{t}} \in [0,1]$, see Fig. 3 (a,b). For $v_{\mathrm{P},21}^{\mathrm{n}} \gg v_{\mathrm{P},21}^{\mathrm{t}}$, the tangential restitution coefficient is obtained as $\epsilon_{\mathrm{t}} = 0$, since we use a lower limit of $\epsilon_{\mathrm{t,min}} = 0$ as proposed in Schwager et al. [17]. Thus, the last case describes a collision in which the total tangential relative velocity vanishes due to friction.

5.1.2. Prolate spheroids

Next, we investigate the influence of the normal and tangential relative particle velocities as well as the aspect ratio $\lambda_1 = a/c$ on the tangential restitution coefficient ϵ_{t}, for prolate ellipsoidal particles, see Fig. 4. Note that for prolate spheroids in centric head-on collision, as in Fig. 2, in Eq. (54) the term $\alpha = \left[1 + m_{\mathrm{eff}} \left[2 I_{zz}^{-1} r_x^2\right]\right]$ can be rewritten in terms of the aspect ratios $\lambda_1 = a/c$ and $\lambda_2 = b/c$. Using that for identical prolate particles in the studied collision configuration $I_{zz} = \frac{1}{5} m \left[a^2 + b^2\right] = \frac{1}{5} m \left[\lambda_1^2 + \lambda_2^2\right] c^2$ and $r_x^2 = a^2 = \lambda_1^2 c^2$, we can write α as

$$\alpha = 1 + \underbrace{m_{\mathrm{eff}}}_{m/2} \left[2 I_{zz}^{-1} \underbrace{r_x^2}_{\lambda_1^2 c^2} \right] = 1 + m \left[\frac{\lambda_1^2 c^2}{\frac{1}{5} m \left[\lambda_1^2 + \lambda_2^2\right] c^2} \right] = 1 + 5 \left[\frac{1}{1 + \lambda_2^2/\lambda_1^2} \right] \,. \tag{55}$$

Note that for prolate spheroids $\lambda_1 > \lambda_2$. Thus, towards strongly elongated particles (i.e. fibers), we obtain $\lambda_2^2/\lambda_1^2 \to 0$ and consequently can write the upper limit as $\alpha_{\mathrm{max}} = 6$. As shown in Fig. 4(a–d), a strong dependence of the tangential restitution coefficient ϵ_{t} on the relative normal ($v_{\mathrm{P},21}^{\mathrm{n}}$) and the relative tangential velocity ($v_{\mathrm{P},21}^{\mathrm{t}}$) as well as the aspect ratio λ_1 can be seen in the case of the studied prolate-ellipsoid particle collision. The general trend of decreasing ϵ_{t} with increasing $v_{\mathrm{P},21}^{\mathrm{n}}$ and increasing ϵ_{t} with decreasing $v_{\mathrm{P},21}^{\mathrm{n}}$ is prevalent similar to the case of spherical particles. Fig. 4(a–d) shows the importance of considering the influence of aspect ratio λ_1 in computing the tangential

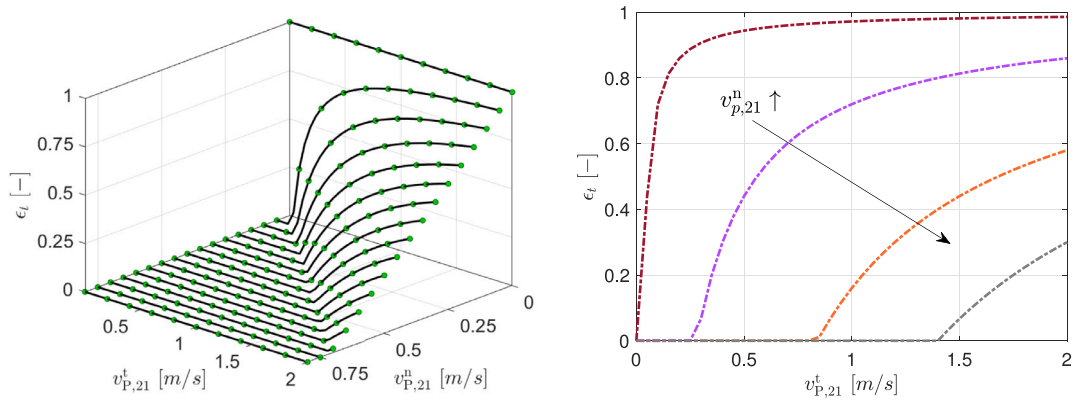

(a) Comparison to Schwager et al., [17] (b) Influence of relative normal velocities $v^{n}_{P,21}$

Fig. 3. The coefficient of tangential restitution ϵ_t for spherical steel particles ($\alpha = 7/2$, $\mu = 0.4$, $\rho_p = 7850$ kg/m^3, $d_{eq} = 0.04$ m) as a function of the relative normal ($v^{n}_{P,21}$) and tangential ($v^{t}_{P,21}$) impact velocity under the assumption of pure Coulomb friction. Schwager et al. [17], present model (Eq. (47)), relative normal velocities $v^{n}_{P,21}$: 0.001, 0.1, 0.3, 0.5.

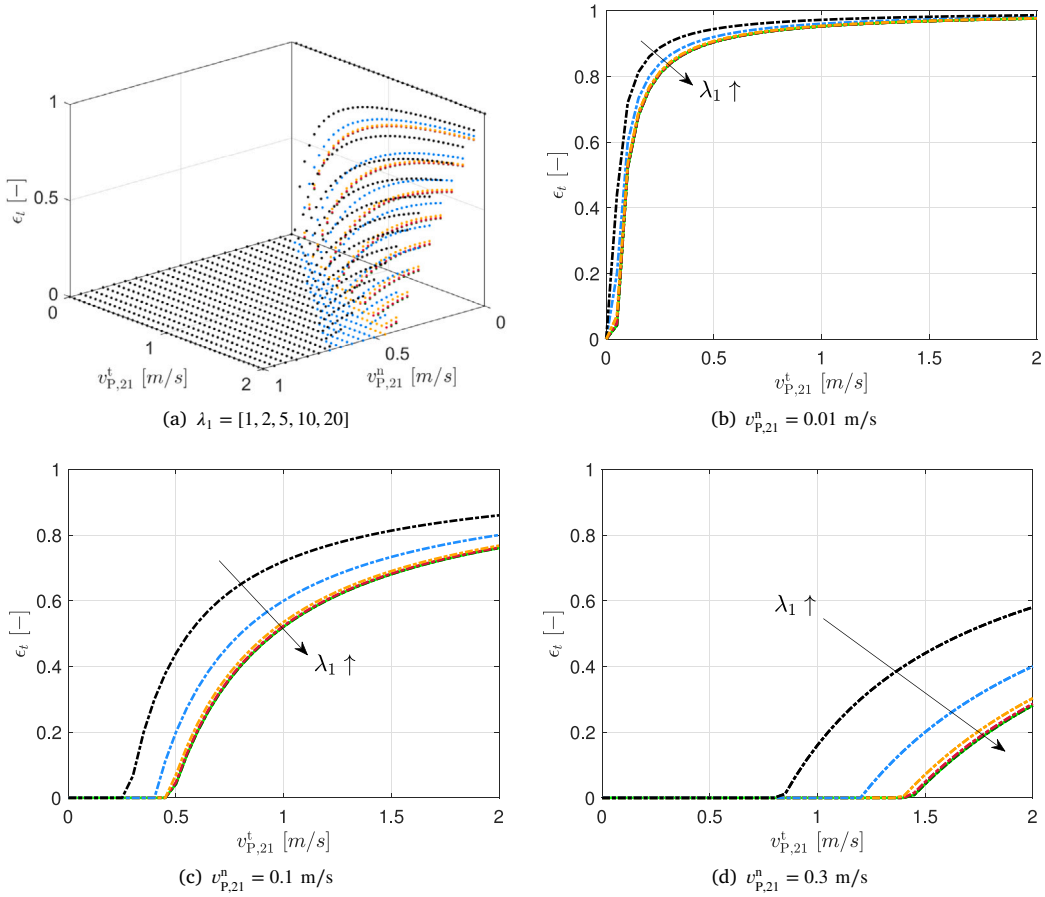

(a) $\lambda_1 = [1, 2, 5, 10, 20]$ (b) $v^{n}_{P,21} = 0.01$ m/s

(c) $v^{n}_{P,21} = 0.1$ m/s (d) $v^{n}_{P,21} = 0.3$ m/s

Fig. 4. The dependency of the coefficient of tangential restitution ϵ_t for spheroidal steel particles ($\lambda_2 = 1$, $s_1 = s_2 = 1$, $\mu = 0.4$, $\rho_p = 7850$ kg/m^3, $d_{eq} = 0.04$ m) as a function of the relative normal ($v^{n}_{P,21}$), tangential ($v^{t}_{P,21}$) impact velocity and aspect ratio (λ_1) under the assumption of pure Coulomb friction. Aspect ratio λ_1: 1, 2, 5, 10, 20, $\lambda_1 \to \infty$ ($\alpha_{max} = 6$).

restitution coefficient ϵ_t, since an increase in λ_1 leads to a significant decrease in ϵ_t. As presented in Fig. 4(a–d), we observe a convergence of ϵ_t towards strongly elongated particles $\lambda_1 \uparrow$, where the coefficient of restitution is bounded by a minimum $\epsilon_{t,min} = f(\alpha_{max} = 6, \ldots)$. Thus, for $\lambda_1 > 5$ the differences in ϵ_t vanish, while for $\lambda_1 < 5$ an accurate consideration of the aspect ratio is required.

5.1.3. Oblate spheroids

In the following, we investigate the influence of the normal and tangential relative particle velocities as well as the aspect ratio $\lambda_1 = \lambda_2$ on the tangential restitution coefficient ϵ_t, for oblate spheroidal particles, see Fig. 5 for $\lambda_1 = \lambda_2 = 5$. When studying the centric head-on collision of two identical oblate spheroids, as shown in Fig. 2, however,

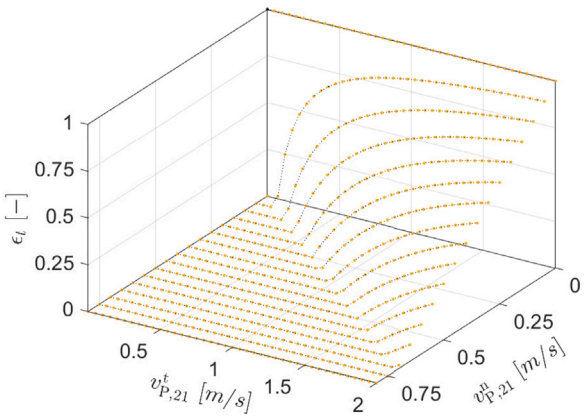

Fig. 5. The coefficient of tangential restitution ϵ_t for steel particles ($\mu = 0.4$, $\rho_p = 7850\ \mathrm{kg/m^3}$, $d_{eq} = 0.04\,\mathrm{m}$) of spherical ($\alpha = 7/2$) and oblate shape ($s_1 = s_2 = 1, \lambda_1 = \lambda_2 = 5$) as a function of the relative normal ($v^n_{P,21}$) and tangential ($v^t_{P,21}$) impact velocity under the assumption of pure Coulomb friction. ▬▮ spherical particles, ● oblate particles.

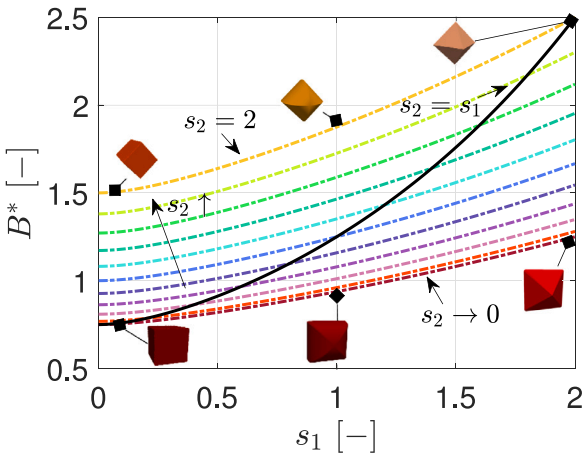

Fig. 6. Dependency of B^* on the squareness parameters s_1 and s_2. ▬ $s_1 = s_2$. $s_2 = [0.0001,\ 0.2,\ 0.4,\ 0.6,\ 0.8,\ 1.0,\ 1.2,\ 1.4,\ 1.6,\ 1.8,\ 2.0]$.

we find that $\alpha = 7/2$. This follows from Eq. (55), using $\lambda_1 = \lambda_2$ (oblate spheroid). The factor α is a constant and thus independent of the aspect ratio $\lambda_1 = \lambda_2$. Consequently, we observe identical ϵ_t for all oblate particles in the studied centrical head-on collision. Fig. 5 highlights that for an oblate particle with arbitrary aspect ratio ($\lambda_1 = \lambda_2 = 5$) we observe identical behavior of the tangential restitution coefficient ϵ_t for varying $v^n_{P,21}$ and $v^t_{P,21}$ than for the spherical case. Thus, as in the case of spherical particle collision, the tangential restitution coefficient ϵ_t depends on the relative normal velocity ($v^n_{P,21}$) and the relative tangential velocity ($v^t_{P,21}$).

5.1.4. Cubical and diamond particles

In the next step, we investigate cubic and diamond particles in the collision configuration depicted in Fig. 2. Note that in the case of cubic and diamond-shaped particles we can additionally study the influence of the shape factors s_1, s_2 on the tangential restitution coefficient, as shown in Fig. 7 and Fig. 8, respectively. Using I_{zz} from Eq. (B.6) as well as the expression for the mass of a superellipsoid particle, see Eq. (B.2), we write:

$$
\begin{aligned}
\alpha =& 1 + \underbrace{m_{\mathrm{eff}}}_{m/2}\left[2 I_{zz}^{-1}\ \underbrace{r_x^2}_{\lambda_1^2 c^2}\right] \\
=& 1 + \left[\frac{m\lambda_1^2 c^2}{\frac{1}{2}\,\rho a\, b\, c\, s_1\, s_2\ \left[a^2+b^2\right]\ \left[B\left(1.5\,s_2, \frac{s_2}{2}\right)\ B\left(\frac{s_1}{2}, 2\,s_1+1\right)\right]}\right] \\
=& 1 + \left[\frac{2\rho abc s_1 s_2 B\left(s_1/2+1, s_1\right) B\left(s_2/2, s_2/2\right) \lambda_1^2 c^2}{\frac{1}{2}\,\rho a\, b\, c\, s_1\, s_2\ \left[a^2+b^2\right]\ \left[B\left(1.5\,s_2, \frac{s_2}{2}\right)\ B\left(\frac{s_1}{2}, 2\,s_1+1\right)\right]}\right] \\
=& 1 + 4\underbrace{\frac{B\left(s_1/2+1, s_1\right) B\left(s_2/2, s_2/2\right)}{B\left(1.5\,s_2, \frac{s_2}{2}\right)\ B\left(\frac{s_1}{2}, 2\,s_1+1\right)}}_{B^*}\left[\frac{\lambda_1^2 c^2}{\left[a^2+b^2\right]}\right] \\
=& 1 + 4B^*\left[\frac{1}{1+\lambda_2^2/\lambda_1^2}\right].
\end{aligned}
\tag{56}
$$

For strongly elongated particles in the studied collision arrangement with $\lambda_1 > \lambda_2$ (prolate particles) we find that $\alpha = 1 + 4B^*$, while for oblate particles ($\lambda_1 = \lambda_2$) we obtain $\alpha = 1 + 2B^*$. Thus, in the range of convex particles $0 \le s_i \le 2.0$, $i = 1, 2$ we obtain B^* values in the range of $B^* = [0.75 - 2.5]$, see Fig. 6. This results in a large variability of the parameter α, see Eq. (56) and consequently renders a strong influence of the particle shape on ϵ_t, see Eq. (54).

Fig. 7 shows a strong dependence of the tangential restitution coefficient ϵ_t on the relative normal ($v^n_{P,21}$) and the relative tangential velocity ($v^t_{P,21}$) as well as the shape factors s_1 and s_2 in the case of the studied cubical–particle collision. In general, an increase in $v^t_{P,21}$ leads still to an increase in ϵ_t. A further increase in ϵ_t can be achieved by decreasing the shape factors $s_1 = s_2$, leading to more cubical particles. For $s_1 = s_2 = 0.001$, i.e. towards sharp cubical shapes, we find that ϵ_t is bounded by a maximum $\epsilon_{t,max} = f(\alpha = 1 + 4B^*)$ with $B^* = 0.075$, see Eq. (56).

Fig. 8 depicts the dependence of the tangential restitution coefficient ϵ_t on the relative normal ($v^n_{P,21}$) and tangential ($v^t_{P,21}$) impact velocities as well as the shape factors $s_1 = s_2$ in the case of the diamond-particle collision studied. Similar to the cubical particles case, an increase in $v^n_{P,21}$ leads to a decreasing ϵ_t, while an increase in $v^t_{P,21}$ leads to an increase in ϵ_t. Moreover, Fig. 8 presents a strong influence of increasing shape factors s_1 and s_2 on ϵ_t, where an increase in shape factors leads to a strong decrease in the tangential coefficient of restitution ϵ_t. As shown in Eq. (56), the tangential restitution coefficient ϵ_t is bounded in the direction of sharp diamond-like convex particles ($s_1 \uparrow$, $s_2 \uparrow$) by a minimum $\epsilon_{t,min} = f(\alpha = 1 + 4B^*)$ with $B^* = 2.5$, see Eq. (56). In the next step, we investigate the influence of the aspect ratio λ_1 by comparing a regular cube and diamond particle ($\lambda_1 = 1$) with a strongly elongated particle version ($\lambda_1 = 20$). In this context, we find that increasing the aspect ratio significantly reduces the tangential restitution coefficient, both for diamond, see Fig. 9(a), as well as for cube-like particles, see Fig. 9(b) for all shape factors studied.

5.2. Collision configuration II

The second collision configuration is shown in Fig. 10, where the particle S_1 is rotated by 90° about the z-axis. The material parameters of the particles remain identical to the collision configuration I, see Section 5.1. With this configuration, we study superellipsoidal particle collisions ranging from oblate and prolate spheroids to cubic and diamond-shaped particles. Note that in this example, the normal velocities are in the $\boldsymbol{e}_1$ direction, while $\boldsymbol{e}_2$ is aligned with the tangential relative velocity $v^t_{P,21}$.

5.2.1. Prolate and oblate spheroids

For prolate and oblate spheroids in centric head-on collision, as depicted in Fig. 10, the term $\alpha = \left[1 + m_{\mathrm{eff}}\left[I_{zz,2}^{-1} r_{x,2}^2 + I_{zz,1}^{-1} r_{x,1}^2\right]\right]$, see Eq. (54), can be rewritten as $I_{zz,2} = 1/5\ m\left[a^2+b^2\right] = I_{zz,1}$, $r_{x,1}^2 = b^2$,

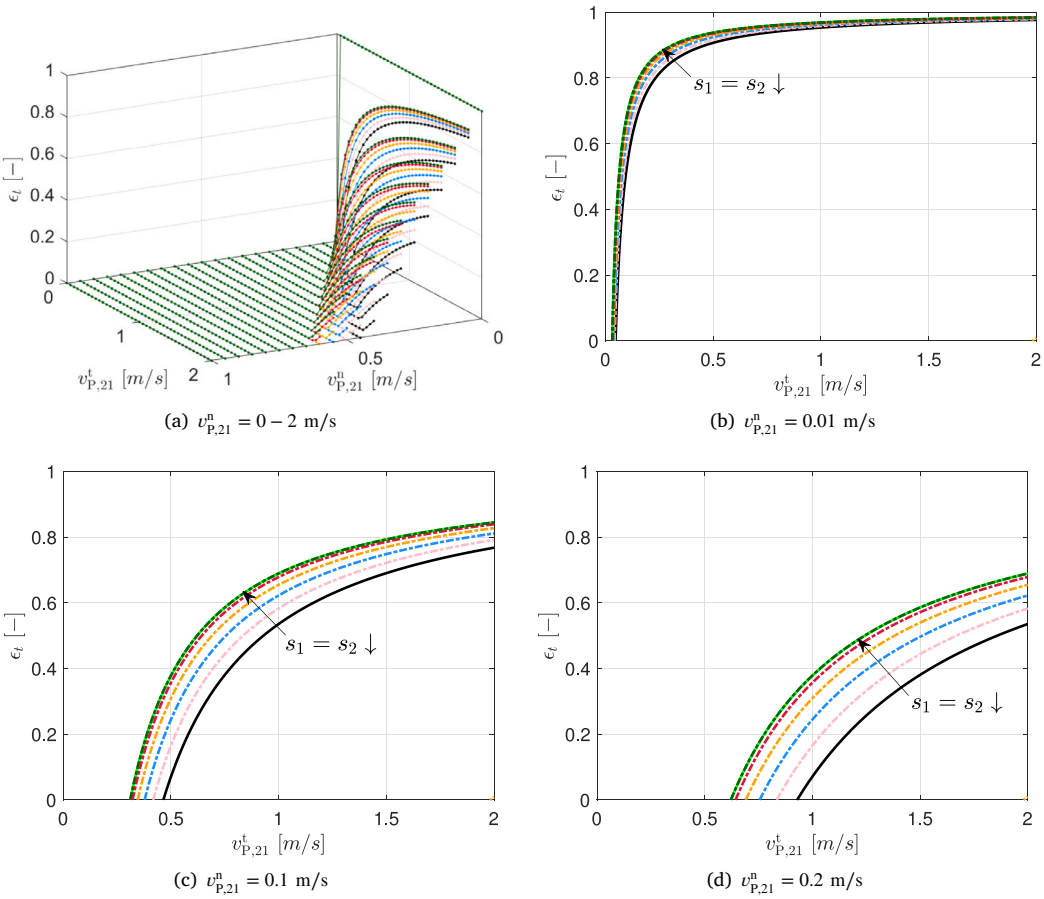

(a) $v^n_{P,21} = 0 - 2$ m/s (b) $v^n_{P,21} = 0.01$ m/s

(c) $v^n_{P,21} = 0.1$ m/s (d) $v^n_{P,21} = 0.2$ m/s

Fig. 7. The coefficient of tangential restitution ϵ_t for a steel particle of cubical shape ($\lambda_1 = 5$, $\lambda_2 = 1.0$, $\mu = 0.4$, $\rho_p = 7850$ kg/m^3, $d_{eq} = 0.04$ m) as a function of the shape factors s_1 (= s_2), relative normal ($v^n_{P,21}$) and tangential ($v^t_{P,21}$) impact velocity under the assumption of pure Coulomb friction. Shape factors $s_1 = s_2$: 1, 0.8, 0.6, 0.4, 0.2, 0.001, $s_1 = s_2 \to 0$ ($B^* = 0.75$).

$r^2_{x,2} = a^2$ for the collision configuration under study, and we obtain

$$\alpha = 1 + \underbrace{m_{\text{eff}}}_{m/2}\left[I^{-1}_{zz,2} r^2_{x,2} + I^{-1}_{zz,1} r^2_{x,1}\right] = 1 + \frac{m}{2}\left[\frac{a^2 + b^2}{\frac{1}{5}\, m\left[a^2 + b^2\right]}\right] = 3.5\,. \quad (57)$$

It follows that $\epsilon_t = \epsilon_{t,\text{sphere}}$ holds for all aspect ratios for both prolate and oblate particles. Consequently, ϵ_t in this collision configuration for oblate and prolate particles depends exclusively on the relative normal ($v^n_{P,21}$) and relative tangential ($v^t_{P,21}$) velocities.

5.2.2. Diamond and cubical particles

In the case of cubic and diamond-shaped particles in the considered collision configuration, see Fig. 10, we find that $\alpha = \left[1 + m_{\text{eff}}\left[I^{-1}_{zz,2} r^2_{x,2} + I^{-1}_{zz,1} r^2_{x,1}\right]\right]$, see Eq. (54), can be rewritten using ($I_{zz} = I_{zz,2} = I_{zz,1}$, $r^2_{x,1} = b^2$, $r^2_{x,2} = a^2$) as well as Eqs. (B.6) and (B.2). This results in:

$$\begin{aligned}\alpha &= 1 + \underbrace{m_{\text{eff}}}_{m/2}\left[I^{-1}_{zz,2} r^2_{x,2} + I^{-1}_{zz,1} r^2_{x,1}\right] \\ &= 1 + \frac{m\left[a^2 + b^2\right]}{2 I_{zz}} \\ &= 1 + 2B^*\,.\end{aligned} \quad (58)$$

As can be seen from Eq. (58), the tangential restitution ϵ_t in the considered collision setup is similar to the oblate and prolate test case independent of the aspect ratio. However, since $B^* = f(s_1, s_2)$ prevails in Eq. (58), an influence of the shape factors on ϵ_t is present for both cubic and diamond-shaped particles. As described in Section 5.1.4, convex particles ($0 \le s_i \le 2.0$, $i = 1, 2$) give $B^* = [0.75 - 2.5]$, see Fig. 6, resulting in large variability of the α parameter in the range of $\alpha = [2.5 - 6]$, see Eq. (58) and consequently a strong influence of the particle shape on ϵ_t, see Eq. (54).

In the first step, the influence of the shape factors for cubical particles ($0 < s_i < 1$, $i = 1, 2$) on the tangential restitution coefficient ϵ_t is investigated. As shown in Fig. 11, similar to collision configuration I (Section 5.1), a decrease in $s_1 \downarrow$, $s_2 \downarrow$ (= towards more cubical shapes) for cubic-shaped particles leads to a higher tangential restitution coefficient, i.e. to a smaller loss of relative tangential velocity during the collision. The upper limit of the tangential restitution coefficient ϵ_t for cubical particles is given by $\epsilon_{t,\max} = f(\alpha = 2.5)$, with $B^* = 0.75$, ($s_1 = s_2 \to 0$), see Eq. (58).

In the second step, we investigate the influence of shape factors on the tangential restitution coefficient in the case of diamond-like particles ($1 < s_i \le 2$, $i = 1, 2$). As shown in Fig. 12, a significant influence of the shape factors on the tangential restitution coefficient ϵ_t remains also for diamond shapes. Similar to the collision configuration I, see Section 5.1, an increase in $s_1 \uparrow$, $s_2 \uparrow$ for diamond-like particles leads to a lower tangential restitution coefficient, i.e. a larger loss of relative tangential velocity during the collision. The lower limit of the tangential restitution coefficient ϵ_t for convex diamond particles is given by $\epsilon_{t,\min} = f(\alpha = 6)$, with $B^* = 2.5$, ($s_1 = s_2 \to 2$), see Eq. (58).

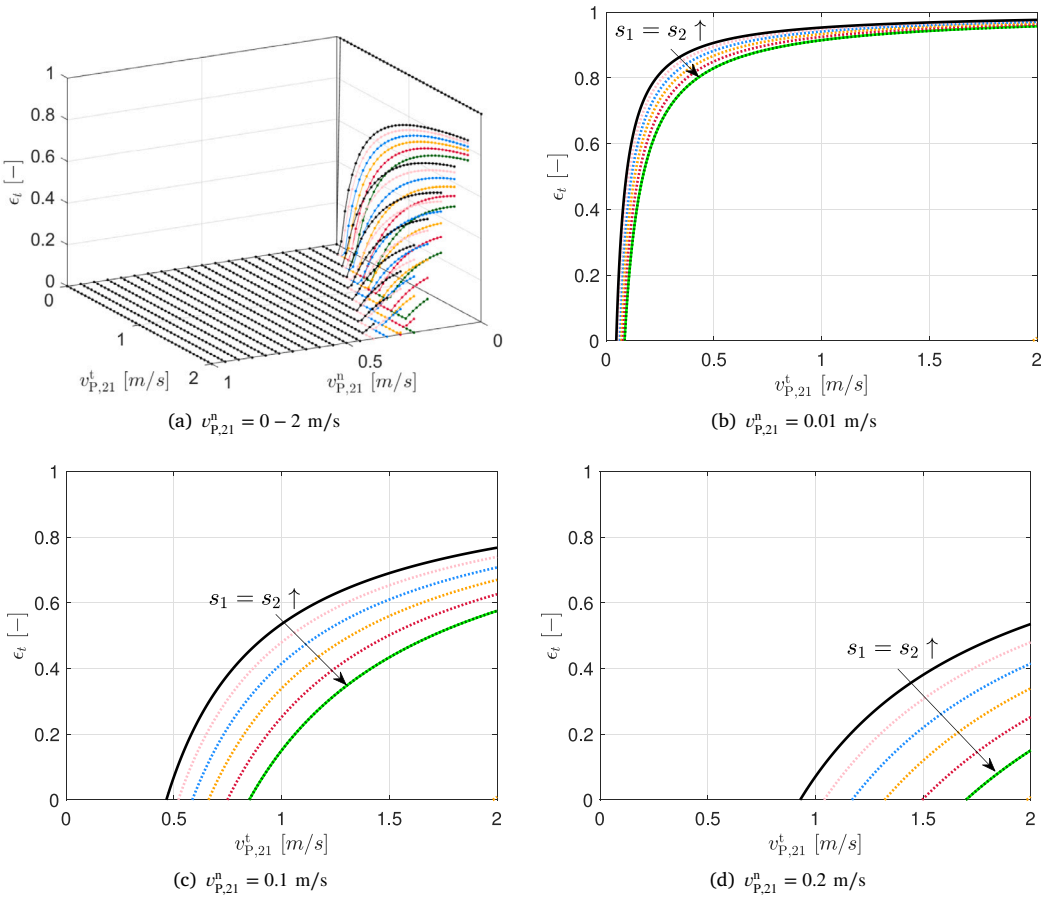

(a) $v^n_{P,21} = 0 - 2$ m/s (b) $v^n_{P,21} = 0.01$ m/s

(c) $v^n_{P,21} = 0.1$ m/s (d) $v^n_{P,21} = 0.2$ m/s

Fig. 8. The coefficient of tangential restitution ϵ_t for a steel particle of diamond shape ($\lambda_1 = 5$, $\lambda_2 = 1$, $\mu = 0.4$, $\rho_p = 7850$ kg/m^3, $d_{eq} = 0.04$ m) as a function of the shape factors s_1 (= s_2), relative normal ($v^n_{P,21}$) and tangential ($v^t_{P,21}$) impact velocity under the assumption of pure Coulomb friction. Shape factors $s_1 = s_2$: 1, 1.2, 1.4, 1.6, 1.8, 2, $s_1 = s_2 \to 2$ ($B^* = 2.5$).

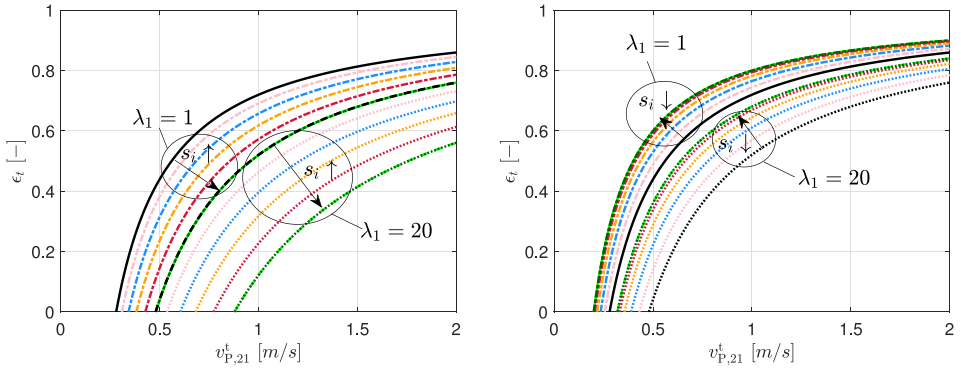

(a) diamond particles (b) cubical particles

Fig. 9. The coefficient of tangential restitution ϵ_t for a steel particle of diamond or cubical shape ($\lambda_2 = 1$, $\mu = 0.4$, $\rho_p = 7850$ kg/m^3, $d_{eq} = 0.04$ m) as a function of the shape factors s_1 (= s_2), relative normal ($v^n_{P,21}$), tangential ($v^t_{P,21}$) impact velocity and aspect ratio (λ_1) under the assumption of pure Coulomb friction. Studied aspect ratios $\lambda_1 = 1$ (striped lines) and $\lambda_1 = 20$ (dotted lines). Shape factors for cubical particles ($s_1 = s_2$): 1, 0.8, 0.6, 0.4, 0.2, 0.001, $s_1 = s_2 \to 0$ ($B^* = 0.75$). Shape factors for diamond-like particles ($s_1 = s_2$): 1, 1.2, 1.4, 1.6, 1.8, 2, $s_1 = s_2 \to 2$ ($B^* = 2.5$).

5.3. Cylinder filling

Finally, examples of cylinder filling with different superellipsoidal particles and friction coefficients μ are studied. The particles are chosen to have size $d_{eq} = 0.01$ m and density $\rho_p = 1000$ kg/m^3. Note that the normal restitution coefficient is chosen to be $\epsilon_n = 0.5$ in all subsequent simulations. We randomly inject 100 particles into a cylinder of $D_{eq} =$ 0.057 m (filled with air at 20 °C) with a minimal initial particle elevation of $2\,d_{eq}$, see Fig. 13. This initialization allows the particles to accelerate after initialization with zero velocity and angular velocity prior to wall contact. First, we study the cylinder filling process with oblate particles ($\lambda_1 = \lambda_2 = 1.5$, $s_1 = s_2 = 1.0$). In this context, we investigate the range of tangential restitution coefficients, i.e. three different cases of ϵ_t, where $\epsilon_t = 1$ refers to no friction, $\epsilon_t = 0$ refers to the complete loss of

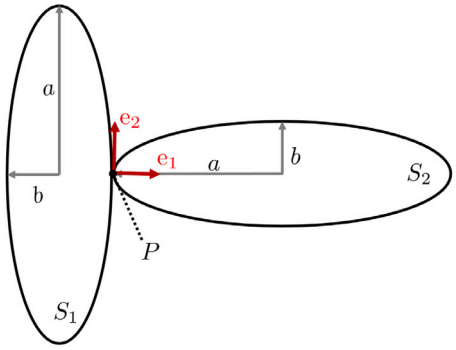

Fig. 10. Sketch of head-on particle collision of two prolate particles (S_1, S_2), where S_1 is rotated by 90° about the z-axis. The half-axis are denoted as a, b, b ($= c$), the collision frame as e_1, e_2 and the contact point as P.

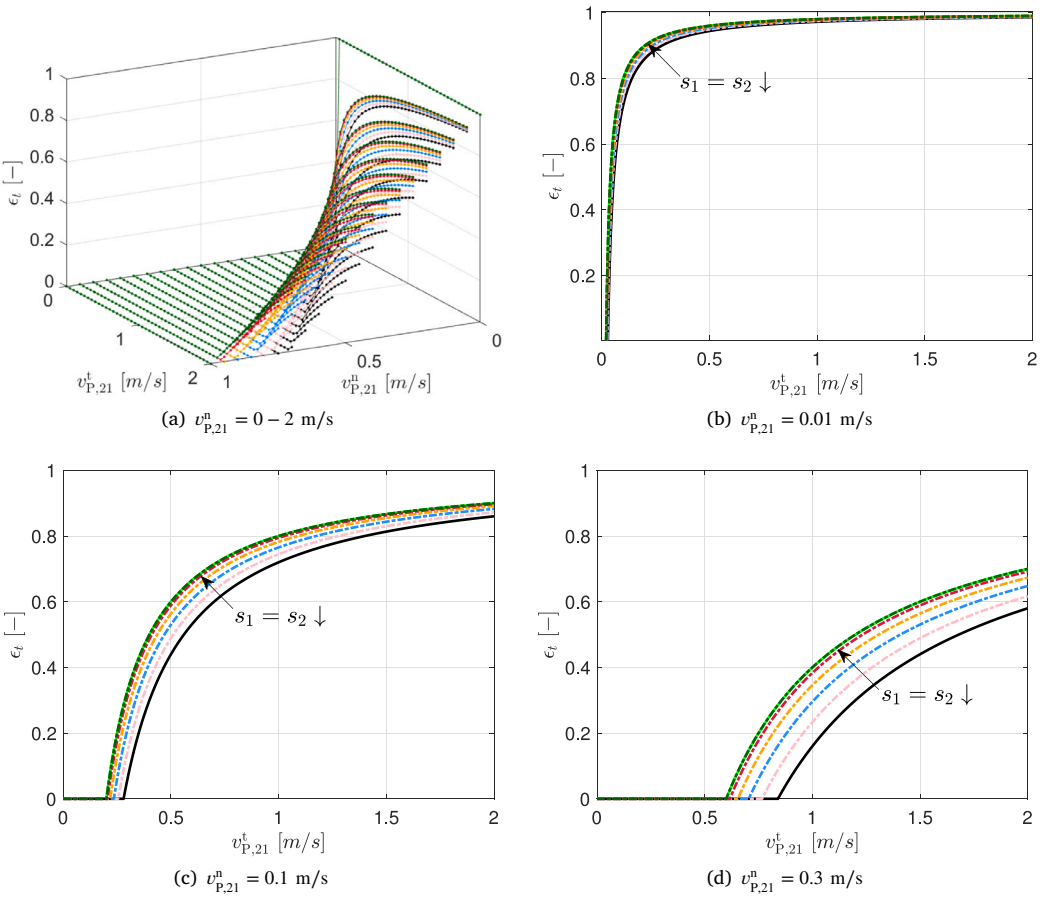

(a) $v^n_{P,21} = 0 - 2$ m/s (b) $v^n_{P,21} = 0.01$ m/s

(c) $v^n_{P,21} = 0.1$ m/s (d) $v^n_{P,21} = 0.3$ m/s

Fig. 11. The coefficient of tangential restitution ϵ_t for a steel particle of cubical shape ($\lambda_1 = \lambda_2 = 1$, $\mu = 0.4$, $\rho_p = 7850$ kg/m^3, $d_{eq} = 0.04$ m) as a function of the shape factors s_1 ($= s_2$), relative normal ($v^n_{P,21}$) and tangential ($v^t_{P,21}$) impact velocity under the assumption of pure Coulomb friction. Shape factors $s_1 = s_2$: 1, 0.8, 0.6, 0.4, 0.2, 0.001, $s_1 = s_2 \to 0$ ($B^* = 0.75$).

the tangential relative velocity after the collision, and an intermediate case that can be obtained by setting the friction coefficient to $\mu = 0.5$, yielding a ϵ_t in the range of $0 \leq \epsilon_t \leq 1$. As shown in Fig. 14, the final stacking height of the considered oblate particles strongly depends on the friction model used. The higher the tangential coefficient of restitution, the lower the volume fraction of the final particle stack. Second, we evaluate the influence of the friction coefficient μ on the stacking height of spherical, oblate ($\lambda_1 = \lambda_2 = 1.5$, $s_1 = s_2 = 1.0$), prolate ($\lambda_1 = 1.5$, $\lambda_2 = 1$, $s_1 = s_2 = 1.0$), cubic ($\lambda_1 = \lambda_2 = 1$, $s_1 = s_2 = 0.6$) as well as diamond-like ($\lambda_1 = \lambda_2 = 1$, $s_1 = s_2 = 1.4$) particles. As presented in Fig. 15, we find a strong dependence of the final packing height on the friction coefficient μ used for all particle shapes considered. We also find that the influence of μ on the packing height is not linear, as the differences between $\mu = 0.1$ and $\mu = 0.25$ are more pronounced than between $\mu = 0.75$ and $\mu = 0.9$. Note that ϵ_t, see Eq. (48), depends also on the normal coefficient of restitution ϵ_n. Thus, increasing ϵ_n would alter the results obtained since it leads to a decrease in ϵ_t.

To estimate the packing density we employ the nondimensional average stacking height $z^* = z/d_{eq}$, see Fig. 16. As presented, for all friction coefficients μ studied, we observe the largest nondimensional average stacking height z^* for spherical particles. With increasing

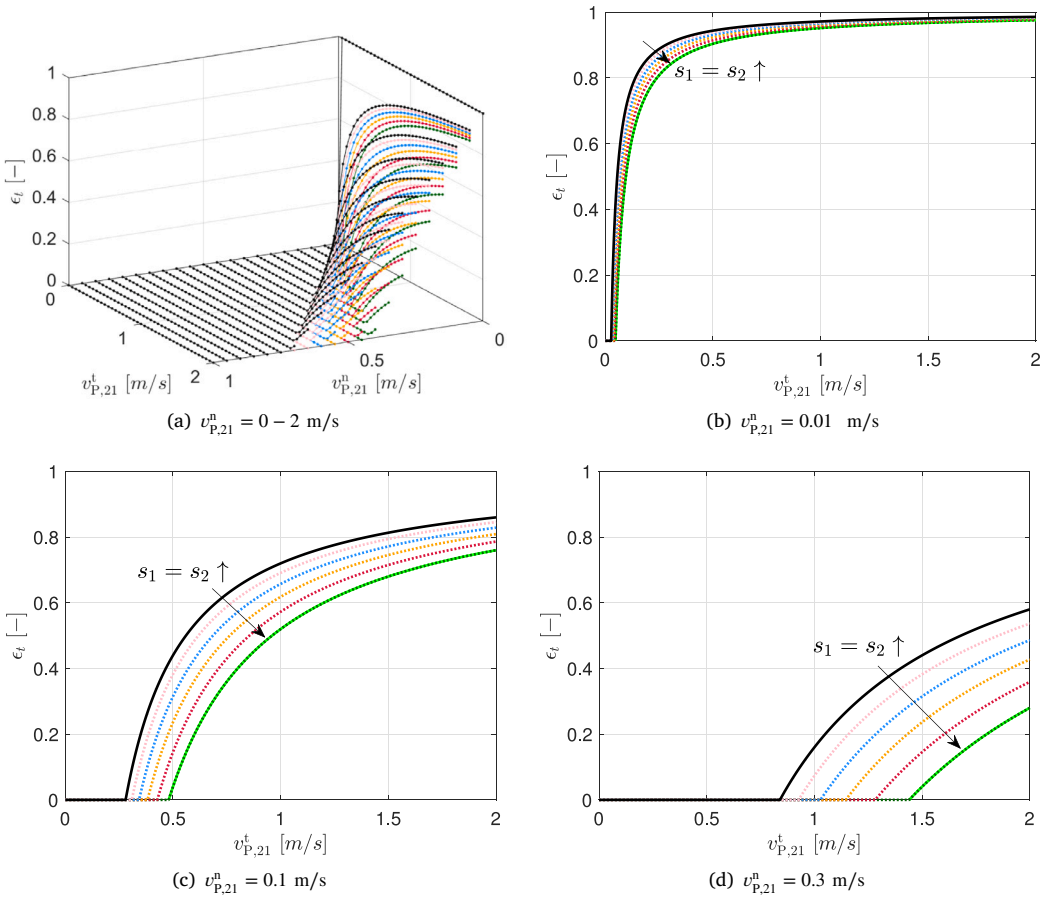

(a) $v^n_{P,21} = 0 - 2$ m/s (b) $v^n_{P,21} = 0.01$ m/s

(c) $v^n_{P,21} = 0.1$ m/s (d) $v^n_{P,21} = 0.3$ m/s

Fig. 12. The coefficient of tangential restitution ϵ_t for a steel particle of diamond shape ($\lambda_1 = \lambda_2 = 1$, $\mu = 0.4$, $\rho_p = 7850$ kg/m^3, $d_{eq} = 0.04$ m) as a function of the shape factors s_1 ($= s_2$), relative normal ($v^n_{P,21}$) and tangential ($v^t_{P,21}$) impact velocity under the assumption of pure Coulomb friction. Shape factors $s_1 = s_2$: 1, 1.2, 1.4, 1.6, 1.8, 2, $s_1 = s_2 \to 2$ ($B^* = 2.5$).

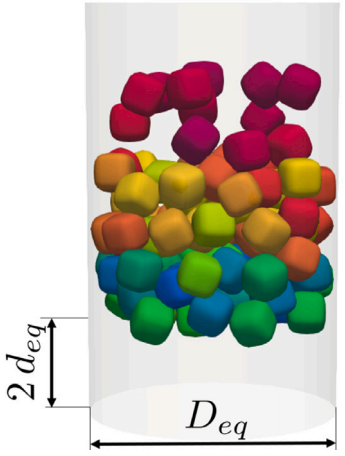

Fig. 13. Sketch of initial position of particles in the cylinder filling simulation.

friction coefficient (up to $\mu = 0.75$) z^* increased for all particles studied, however, note the non-linear trend. Moreover, we observe that the lowest z^* and thus the highest packing density is obtained using cubical particles for all investigated friction coefficients. Furthermore, we observe that the difference between the stacking heights of the shapes is the highest for the lowest friction coefficient $\mu = 0.1$ studied.

Note that by only slightly varying the particle shape from the spherical shapes, see the oblate ($\lambda_1 = \lambda_2 = 1.5$, $s_1 = s_2 = 1$), prolate ($\lambda_1 = 1.5$, $\lambda_2 = s_1 = s_2 = 1$), diamond-like ($\lambda_1 = \lambda_2 = 1$, $s_1 = s_2 = 1.4$), and cubical particles ($\lambda_1 = \lambda_2 = 1$, $s_1 = s_2 = 0.6$) considered, we observe significant differences in particle stack (Fig. 15) as well as in average particle heights (Fig. 16). Thus, we emphasize the importance of considering the dependence of the tangential coefficient of restitution on particle shape as deviations from the spherical reference occur.

6. Conclusion

In this article, we proposed a novel model of the tangential restitution coefficient as an extension of our previously presented efficient computation of three-dimensional frictional collisions between particles and between particles and walls based on a superellipsoidal particle shape definition using a robust Newton–Raphson based Lagrangian multiplier optimization technique. This work aimed to extend the previously used simplified friction model, where only a fixed tangential restitution coefficient ϵ_t or spherical models were available for non-spherical particles.

We present the derivation of the tangential coefficient of restitution for arbitrarily shaped particles based on the assumption of Coulomb friction. Thus, the model assumes pure sliding between the collision partners, i.e. $\epsilon_t \geq 0$. Furthermore, we assume a constant ϵ_n as commonly employed in the literature. In addition, we validated the novel collision model for non-spherical particles against literature results for spherical particles in Coulomb friction. In addition, we performed examples of

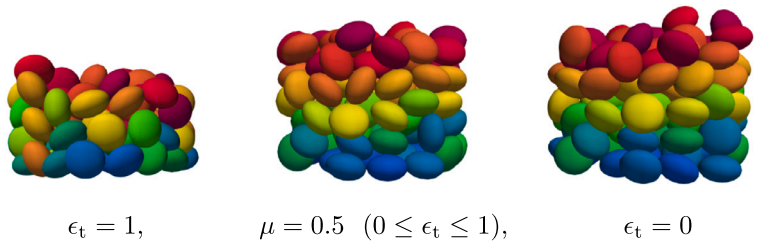

Fig. 14. Comparison of fixed tangential restitution coefficient ϵ_t (left, right) to novel frictional collision model (middle).

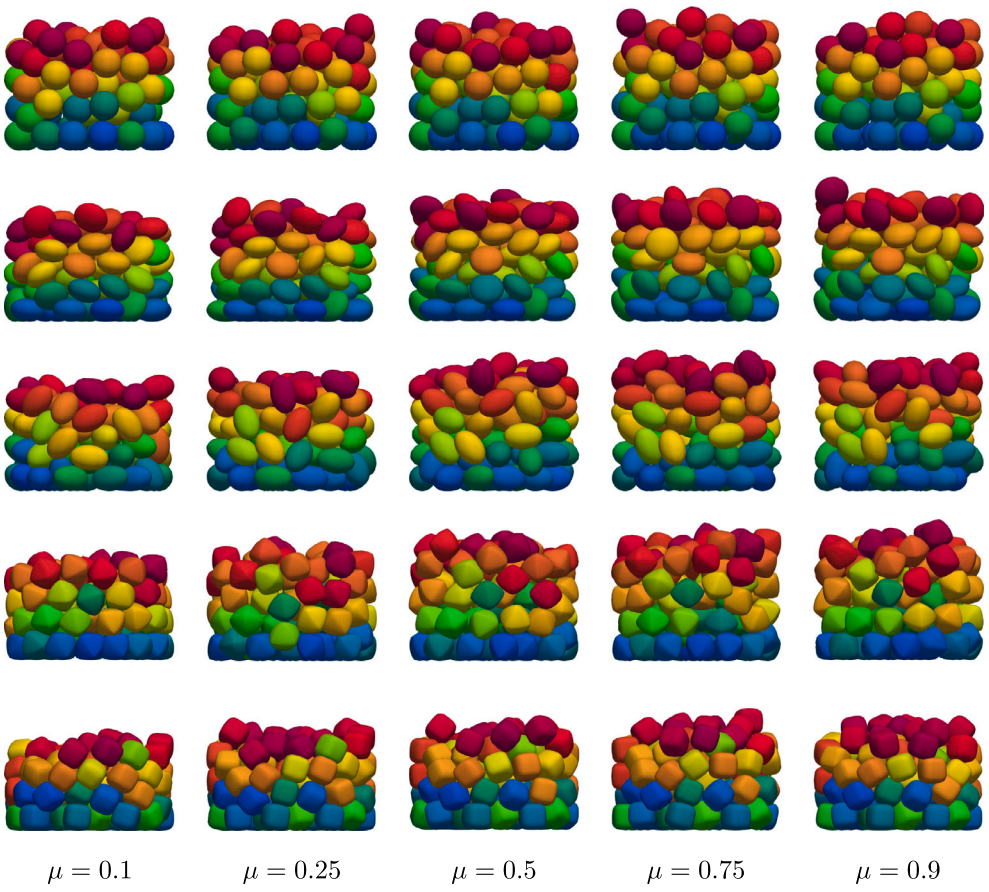

Fig. 15. Influence of the friction coefficient μ on the final packing of spherical, oblate ($\lambda_1 = \lambda_2 = 1.5$), prolate ($\lambda_1 = 1.5,\ \lambda_2 = 1$), diamond-like ($\lambda_1 = 1.5,\ \lambda_2 = 1,\ s_1 = s_2 = 1.4$) and cubical particles ($\lambda_1 = 1.5,\ \lambda_2 = 1,\ s_1 = s_2 = 0.6$) using $\epsilon_n = 0.5$.

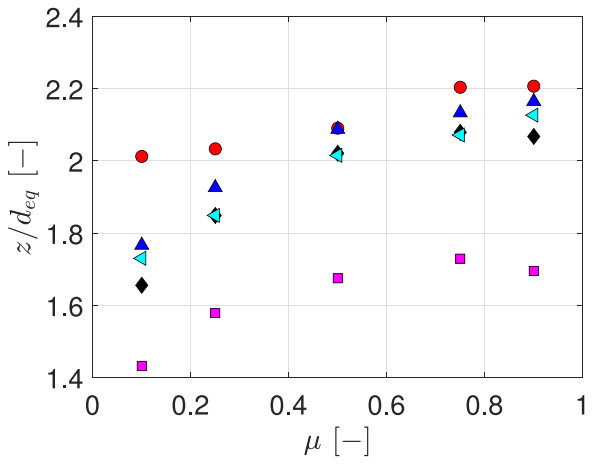

Fig. 16. Average dimensionless stacking height $z^* = z/d_{eq}$ of various superellipsoidal particles: ● spheres, ◁ oblate ellipsoids ($\lambda_1 = \lambda_2 = 1.5$) ▲ prolate ellipsoids ($\lambda_1 = 1.5$, $\lambda_2 = 1$), ◆ diamond-like particles, ■ cubical particles.

cylinder filling simulations, where we investigated different particle shapes from oblate to cubes to diamond-like shapes, as well as different coefficients of friction (μ). By varying the shapes slightly from the spherical reference, we were able to establish the importance of considering the dependence of the tangential coefficient of restitution on particle shape as deviations from the spherical reference occur. The derived superellipsoidal particle contact model including the improved friction treatment can be directly applied in CFD with Lagrangian particle tracking algorithms. In our future work, we intend to extend our tangential restitution coefficient model for arbitrary particles by incorporating different force laws. Furthermore, we aim to apply the novel friction model for non-spherical particles to study more complex phenomena of particles transported in flows.

CRediT authorship contribution statement

Jana Wedel: Writing – review & editing, Writing – original draft, Visualization, Validation, Software, Methodology, Investigation, Formal analysis, Data curation, Conceptualization. **Matjaž Hriberšek:** Writing – review & editing, Supervision, Resources, Methodology, Formal analysis, Conceptualization. **Paul Steinmann:** Writing – review & editing, Supervision, Resources, Project administration, Methodology, Funding acquisition, Formal analysis, Conceptualization. **Jure Ravnik:** Writing – review & editing, Supervision, Resources, Methodology, Formal analysis, Conceptualization.

Declaration of competing interest

The authors declare that they have no known competing financial interests or personal relationships that could have appeared to influence the work reported in this paper.

Data availability

Data will be made available on request.

Acknowledgments

The authors thank the Deutsche Forschungsgemeinschaft for the financial support in the framework of the project STE 544/75-1 and the Slovenian Research and Innovation Agency (research core funding No. P2-0196).

Appendix A. Notation

In the following, tensors of various orders are denoted using bold italic font. Note that vectors (first-order tensors) are expressed using bold italic lowercase letters ($\boldsymbol{a}$), while higher-order tensors are denoted by bold italic uppercase letters ($\boldsymbol{A}$). The coordinate representation of two Cartesian coordinate systems with base vectors $\boldsymbol{e}'_i$, $\boldsymbol{e}_i$ ($i = 1,2,3$) can be written using Einstein's summation convention, as follows:

$$\boldsymbol{a} = a'_i \boldsymbol{e}'_i = a_i \boldsymbol{e}_i \quad \text{and} \quad \boldsymbol{A} = A'_{ij} \boldsymbol{e}'_i \otimes \boldsymbol{e}'_j = A_{ij} \boldsymbol{e}_i \otimes \boldsymbol{e}_j .$$

In this context, a'_i, a_i and A'_{ij}, A_{ij} represent the corresponding tensor coefficients in the coordinate system $\boldsymbol{e}'_i$, $\boldsymbol{e}_i$, respectively. The coefficient matrices a'_i, a_i and A'_{ij}, A_{ij} are expressed by underlined italic letters:

$$\underline{a}' = \begin{bmatrix} a'_1 \\ a'_2 \\ a'_3 \end{bmatrix}, \quad \underline{a} = \begin{bmatrix} a_1 \\ a_2 \\ a_3 \end{bmatrix} \quad \text{and} \quad \underline{A}' = \begin{bmatrix} A'_{11} & A'_{12} & A'_{13} \\ A'_{21} & A'_{22} & A'_{23} \\ A'_{31} & A'_{32} & A'_{33} \end{bmatrix},$$

$$\underline{A} = \begin{bmatrix} A_{11} & A_{12} & A_{13} \\ A_{21} & A_{22} & A_{23} \\ A_{31} & A_{32} & A_{33} \end{bmatrix}.$$

The rotation matrix $\underline{R}$ relating the coordinate systems $\boldsymbol{e}'_i$, $\boldsymbol{e}_i$ is given as

$$\underline{R} = \begin{bmatrix} R_{11} & R_{12} & R_{13} \\ R_{21} & R_{22} & R_{23} \\ R_{31} & R_{32} & R_{33} \end{bmatrix} \quad \text{with} \quad R_{ij} = \boldsymbol{e}'_i \cdot \boldsymbol{e}_j \tag{A.1}$$

and transforms coefficients with respect to the base vectors $\boldsymbol{e}_i$ to coefficients with respect to $\boldsymbol{e}'_i$. Using $\underline{R}$, we can transform coefficient matrices of vectors and second-order tensors in the following manner

$$\underline{a}' = \underline{R}\,\underline{a} \quad \text{and} \quad \underline{A}' = \underline{R}\,\underline{A}\,\underline{R}^{\mathrm{T}} . \tag{A.2}$$

Appendix B. Surface equation of a superellipsoid

To describe non-spherical particles, we employ the superellipsoid surface equation as proposed by Barr, [48]. This surface equation reads in the particle frame of reference (pFoR) $[x', y', z']$ as

$$S(x', y', z') = \left[\left[\frac{|x'|}{a} \right]^{2/s_2} + \left[\frac{|y'|}{b} \right]^{2/s_2} \right]^{s_2/s_1} + \left[\frac{|z'|}{c} \right]^{2/s_1} - 1 = 0 , \tag{B.1}$$

where the particle half-lengths in the direction of the principle axes are denoted as a, b and c. In this work, we set $c \le b \le a$ and express the aspect ratios as $\lambda_1 = a/c \ge \lambda_2 = b/c$. The shape factors s_1 and s_2 control the squareness of the particle, [7,8]. The mass of a superellipsoidal particle can be written as: [49]

$$m = 2\rho_p abc s_1 s_2 B\left(\frac{s_1}{2} + 1, s_1\right) B\left(\frac{s_2}{2}, \frac{s_2}{2}\right) , \tag{B.2}$$

where ρ_p denotes the particle density. Furthermore, B is related to the Gamma function as follows: [49]

$$B(x, y) = \frac{\Gamma(x)\Gamma(y)}{\Gamma(x + y)} . \tag{B.3}$$

In Fig. B.17 a set of representative superellipsoidal particles is displayed. The principal values of the inertia tensor of the particle are denoted by I'_{xx}, I'_{yy}, I'_{zz}. The expressions of the principal values of the inertia tensor for a superellipsoidal particle are: [49]

$$I'_{xx} = \frac{1}{2}\rho abc s_1 s_2 \left[b^2 B\left(1.5 s_2, \frac{s_2}{2}\right) B\left(\frac{s_1}{2}, 2s_1 + 1\right) + 4c^2 B\left(\frac{s_2}{2}, \frac{s_2}{2} + 1\right) B\left(1.5 s_1, s_1 + 1\right) \right] , \tag{B.4}$$

$$I'_{yy} = \frac{1}{2}\rho abc s_1 s_2 \left[a^2 B\left(1.5 s_2, \frac{s_2}{2}\right) B\left(\frac{s_1}{2}, 2s_1 + 1\right) + 4c^2 B\left(\frac{s_2}{2}, \frac{s_2}{2} + 1\right) B\left(1.5 s_1, s_1 + 1\right) \right] , \tag{B.5}$$

$$I'_{zz} = \frac{1}{2}\,\rho\, a\, b\, c\, s_1\, s_2\, \left[a^2 + b^2\right] \left[B\left(1.5\, s_2, \frac{s_2}{2}\right)\, B\left(\frac{s_1}{2}, 2\, s_1 + 1\right) \right] . \tag{B.6}$$

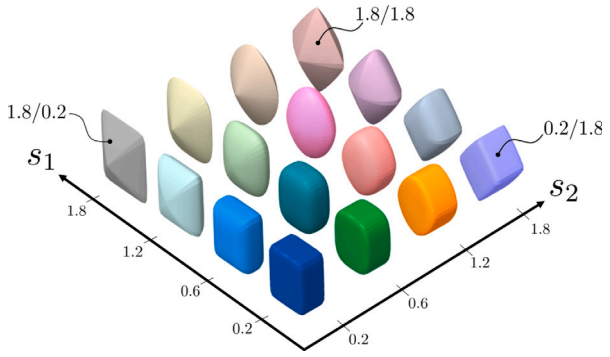

Fig. B.17. Representative superellipsoidal shapes with $\lambda_1 > \lambda_2$ and varying shape factors $s_1, s_2 = [0.2, 1.8]$.

Appendix C. Particle–wall collision

In the case of particle–wall collision, γ, see Eq. (42), simplifies to

$$\gamma_{wall} = m\left[-\Delta\tilde{\boldsymbol{\omega}} \times \boldsymbol{r}^*\right] \cdot \boldsymbol{e}_{\mathrm{n}} \tag{C.1}$$

and β, see Eq. (45), to

$$\beta_{wall} = m\left[-\Delta\tilde{\boldsymbol{\omega}} \times \boldsymbol{r}^*\right] \cdot \boldsymbol{e}_{\mathrm{t}}\,. \tag{C.2}$$

Consequently, we obtain the final expression for the tangential restitution coefficient ϵ_{t} for arbitrarily shaped particles in collision with walls under the assumption of Coulomb friction by inserting the expressions of $\gamma = \gamma_{wall}$ and $\beta = \beta_{wall}$ into Eq. (48).

References

[1] P.W. Cleary, G.W. Delaney, M.D. Sinnott, S.J. Cummins, R.D. Morrison, Advanced comminution modelling: Part 1 – Crushers, Appl. Math. Model. 88 (2020) 238–265, http://dx.doi.org/10.1016/j.apm.2020.06.049.

[2] Y. Cui, J. Ravnik, P. Steinmann, M. Hriberšek, Settling characteristics of nonspherical porous sludge flocs with nonhomogeneous mass distribution, Water Res. 158 (2019) 159–170.

[3] K. Ahookhosh, M. Saidi, H. Aminfar, M. Mohammadpourfard, H. Hamishehkar, S. Yaqoubi, Dry powder inhaler aerosol deposition in a model of tracheobronchial airways: Validating CFD predictions with in vitro data, Int. J. Pharm. 587 (2020) 119599, http://dx.doi.org/10.1016/j.ijpharm.2020.119599.

[4] C. Hogue, D. Newland, Efficient computer simulation of moving granular particles, Powder Technol. 78 (1994) 51–66, http://dx.doi.org/10.1016/0032-5910(93)02748-Y.

[5] Y. Feng, D. Owen, A 2D polygon/polygon contact model: Algorithmic aspects, Eng. Comput. 21 (2004) 265–277, http://dx.doi.org/10.1108/02644400410519785.

[6] J.R. Williams, R. O'Connor, Discrete element simulation and the contact problem, Arch. Comput. Methods Eng. 6 (4) (1999) 279–304, http://dx.doi.org/10.1007/BF02818917.

[7] G. Lu, J. Third, C. Müller, Critical assessment of two approaches for evaluating contacts between super-quadric shaped particles in DEM simulations, Chem. Eng. Sci. 78 (2012) 226–235, http://dx.doi.org/10.1016/j.ces.2012.05.041.

[8] Y. You, Y. Zhao, Discrete element modelling of ellipsoidal particles using super-ellipsoids and multi-spheres : A comparative study, Powder Technol. 331 (2018) 179–191, http://dx.doi.org/10.1016/j.powtec.2018.03.017.

[9] J. Wedel, M. Štrakl, P. Steinmann, M. Hriberšek, J. Ravnik, A novel particle-particle and particle-wall collision model for superellipsoidal particles, Comput. Part. Mech. (2023) http://dx.doi.org/10.1007/s40571-023-00618-6.

[10] G.G.W. Mustoe, M. Miyata, Material Flow Analyses of Noncircular-Shaped Granular Media Using Discrete Element Methods, Tech. Rep. 10, 2001, pp. 1017–1026, http://dx.doi.org/10.1061/(asce)0733-9399(2001)127:10(1017).

[11] C. Hogue, Shape representation and contact detection for discrete element simulations of arbitrary geometries, Eng. Comput. (Swansea, Wales) 15 (2–3) (1998) 374–390, http://dx.doi.org/10.1108/02644409810208525.

[12] J. Favier, M. Abbaspour-Fard, M. Kremmer, A. Raji, Shape representation of axi-symmetrical, non-spherical particles in discrete element simulation using multi-element model particles, Eng. Comput. 16 (4) (1999) 467–480.

[13] R. Jensen, P. Bosscher, M. Plesha, T. Edil, DEM Simulation of granular media - structure interface: effects of surface roughness and particle shape, Int. J. Numer. Anal. Methods Geomech. 23 (1999) 531–547.

[14] M. Abbaspour-Fard, Theoretical validation of a multi-sphere, discrete element model suitable for biomaterials handling simulation, Biosyst. Eng. 88 (2) (2004) 153–161, http://dx.doi.org/10.1016/j.biosystemseng.2004.03.010.

[15] T. Schwager, T. Pöschel, Coefficient of normal restitution of viscous particles and cooling rate of granular gases, Phys. Rev. E 57 (1) (1998) 650–654, http://dx.doi.org/10.1103/PhysRevE.57.650.

[16] M. Hu, Y.J. Huang, F. Wang, M.S. Foss, The Coefficient of Restitution of Spheroid Particles Impacting on a Wall—Part I: Experiments, J. Appl. Mech. 85 (4) (2018) 041006, http://dx.doi.org/10.1115/1.4038920.

[17] T. Schwager, V. Becker, T. Pöschel, Coefficient of tangential restitution for viscoelastic spheres, Eur. Phys. J. E 27 (2008) 107–114, http://dx.doi.org/10.1140/epje/i2007-10356-3.

[18] V. Becker, T. Schwager, T. Pöschel, Coefficient of tangential restitution for the linear dashpot model, Phys. Rev. E 77 (2008) 011304, http://dx.doi.org/10.1103/PhysRevE.77.011304.

[19] F. Bridges, A. Hatzes, D. Lin, Structure, stability and evolution of saturn's rings, Nature 309 (1984) 333–335, http://dx.doi.org/10.1038/309333a0.

[20] J. McDonald, A. Hatzes, F. Bridges, D. Lin, Mass transfer during ice particle collisions in planetary rings, Icarus 82 (1) (1989) 167–179, http://dx.doi.org/10.1016/0019-1035(89)90029-8.

[21] F.G. Bridges, K.D. Supulver, D. Lin, R. Knight, M. Zafra, Energy loss and sticking mechanisms in particle aggregation in planetesimal formation, Icarus 123 (2) (1996) 422–435, http://dx.doi.org/10.1006/icar.1996.0168.

[22] T. Kane, A dynamics puzzle, Stanf. Mech. Alumni Club News Lett. 6 (1984) 1–4.

[23] Y. Huang, M. Hu, T. Zhou, Modelling of the coefficients of restitution for prolate spheroid particles and its application in simulations of 2D granular flow, Granul. Matter 24 (83) (2022) http://dx.doi.org/10.1007/s10035-022-01241-7.

[24] N. Gui, X. Yang, J. Tu, S. Jiang, A generalized particle-to-wall collision model for non-spherical rigid particles, Adv. Powder Technol. 27 (1) (2016) 154–163, http://dx.doi.org/10.1016/j.apt.2015.12.002.

[25] M. Štrakl, M. Hriberšek, J. Wedel, P. Steinmann, J. Ravnik, A model for translation and rotation resistance tensors for superellipsoidal particles in Stokes flow, J. Mar. Sci. Eng. 10 (3) (2022) 369.

[26] Y.-h. Taguchi, New origin of a convective motion: Elastically induced convection in granular materials, Phys. Rev. Lett. 69 (9) (1992) 1367–1370, http://dx.doi.org/10.1103/PhysRevLett.69.1367.

[27] J.A.C. Gallas, H.J. Herrmann, S. Sokołowski, Convection cells in vibrating granular media, Phys. Rev. Lett. 69 (9) (1992) 1371–1374, http://dx.doi.org/10.1103/PhysRevLett.69.1371, URL https://link.aps.org/doi/10.1103/PhysRevLett.69.1371.

[28] L.E. Silbert, D. Ertaş, G.S. Grest, T.C. Halsey, D. Levine, Geometry of frictionless and frictional sphere packings, Phys. Rev. E 65 (2002) 031304, http://dx.doi.org/10.1103/PhysRevE.65.031304, URL https://link.aps.org/doi/10.1103/PhysRevE.65.031304.

[29] L.S. Tsimring, D.N. Volfson, Modeling of impact cratering in granular media, in: Powders and Grains, 2005, pp. 1215–1223.

[30] S. Luding, Stress distribution in static two-dimensional granular model media in the absence of friction, Phys. Rev. E 55 (4) (1997) 4720–4729, http://dx.doi.org/10.1103/PhysRevE.55.4720, URL https://link.aps.org/doi/10.1103/PhysRevE.55.4720.

[31] S. Luding, E. Clément, A. Blumen, J. Rajchenbach, J. Duran, Onset of convection in molecular dynamics simulations of grains, Phys. Rev. E 50 (3) (1994) R1762–R1765.

[32] O. Mouraille, W. Mulder, S. Luding, Sound wave acceleration in granular materials, J. Stat. Mech. Theory Exp. 2006 (2006) http://dx.doi.org/10.1088/1742-5468/2006/07/P07023.

[33] L. Oger, S. Savage, D. Corriveau, M. Sayed, Yield and deformation of an assembly of disks subjected to a deviatoric stress loading, Mech. Mater. 27 (4) (1998) 189–210, http://dx.doi.org/10.1016/S0167-6636(97)00066-5.

[34] J. Schäfer, D.E. Wolf, Bistability in simulated granular flow along corrugated walls, Phys. Rev. E 51 (6) (1995) 6154–6157, http://dx.doi.org/10.1103/PhysRevE.51.6154.

[35] P.A. Thompson, G.S. Grest, Granular flow: Friction and the dilatancy transition, Phys. Rev. Lett. 67 (13) (1991) 1751–1754, http://dx.doi.org/10.1103/PhysRevLett.67.1751.

[36] G. Weir, S. Tallon, The coefficient of restitution for normal incident, low velocity particle impacts, Chem. Eng. Sci. 60 (13) (2005) 3637–3647, http://dx.doi.org/10.1016/j.ces.2005.01.040.

[37] S. Luding, E. Clément, A. Blumen, J. Rajchenbach, J. Duran, Anomalous energy dissipation in molecular-dynamics simulations of grains: The "detachment" effect, Phys. Rev. E 50 (5) (1994) 4113–4122, http://dx.doi.org/10.1103/PhysRevE.50.4113.

[38] R. Ramírez, T. Pöschel, N.V. Brilliantov, T. Schwager, Coefficient of restitution of colliding viscoelastic spheres, Phys. Rev. E 60 (4) (1999) 4465–4472, http://dx.doi.org/10.1103/PhysRevE.60.4465.

[39] Y. Tsuji, T. Tanaka, T. Ishida, Lagrangian numerical simulation of plug flow of cohesionless particles in a horizonal pipe, Powder Technol. 71 (3) (1992) 239–250, http://dx.doi.org/10.1016/0032-5910(92)88030-L.

[40] W. Ludwig, P. Pluszka, Euler-Lagrange model of particles circulation in a spout-fluid bed apparatus for dry coating, Powder Technol. 328 (2018) 375–388, http://dx.doi.org/10.1016/j.powtec.2018.01.032.

[41] W. Ludwig, P. Pluszka, The analysis of the influence of the normal restitution coefficient model on calculated particles velocities by means of Eulerian-Lagrangian approach, Powder Technol. 344 (2019) 140–151, http://dx.doi.org/10.1016/j.powtec.2018.12.004.

[42] J. Shäfer, S. Dippel, D.E. Wolf, Force schemes in simulations of granular materials, J. Physique I 6 (1) (1996) 5–20, URL https://api.semanticscholar.org/CorpusID:58925026.

[43] A. Stevens, C. Hrenya, Comparison of soft-sphere models to measurements of collision properties during normal impacts, Powder Technol. 154 (2) (2005) 99–109, http://dx.doi.org/10.1016/j.powtec.2005.04.033, URL https://www.sciencedirect.com/science/article/pii/S0032591005001658.

[44] H. Kruggel-Emden, E. Simsek, S. Rickelt, S. Wirtz, V. Scherer, Review and extension of normal force models for the discrete element method, Powder Technol. 171 (3) (2007) 157–173, http://dx.doi.org/10.1016/j.powtec.2006.10.004, URL https://www.sciencedirect.com/science/article/pii/S0032591006004360.

[45] P. Haff, B. Werner, Computer simulation of the mechanical sorting of grains, Powder Technol. 48 (3) (1986) 239–245, http://dx.doi.org/10.1016/0032-5910(86)80048-1.

[46] P.A. Cundall, O.D.L. Strack, A discrete numerical model for granular assemblies, Géotechnique 29 (1) (1979) 47–65, http://dx.doi.org/10.1680/geot.1979.29.1.47.

[47] C. Thornton, S.J. Cummins, P.W. Cleary, An investigation of the comparative behaviour of alternative contact force models during inelastic collisions, Powder Technol. 233 (2013) 30–46, http://dx.doi.org/10.1016/j.powtec.2012.08.012.

[48] A.H. Barr, Superquadrics and angle-preserving transformations, IEEE Comput. Graph. Appl. 1 (1) (1981) 11–23.

[49] A. Jaklič, A. Leonardis, F. Solina, Superquadrics and Their Geometric Properties, vol. 20, 2000, pp. 13–39, http://dx.doi.org/10.1007/978-94-015-9456-1_2.